

This is a non-peer-reviewed preprint submitted to EarthArxiv, which was submitted to Geochemical Perspectives Letters on September 20th, 2023.

Reliability of Raman analyses of CO₂-rich fluid inclusions as a rapid barometer at Kīlauea

Charlotte L. Devitre¹, Penny E. Wieser¹

¹ University of California, Berkeley, Berkeley, CA 94270

We hope that this will inspire new work using FI barometry! We welcome constructive feedback, please reach out to cl.devitre@gmail.com. If our stretching tool is not working for you, please reach out or raise an issue on Github (<https://github.com/cljdevitre/RelaxiFI/issues>)!

RELIABILITY OF RAMAN ANALYSES OF CO₂-RICH FLUID INCLUSIONS AS A RAPID BAROMETER AT KĪLAUEA

CHARLOTTE L. DEVITRE^{1,*} AND PENNY E. WIESER¹

¹*Earth and Planetary Sciences, University of California, Berkeley, Berkeley, 94720, CA, USA*

**cl.devitre@gmail.com*

Submitted to *Geochemical Perspectives Letters* on September 20, 2023

ABSTRACT

Interpreting signals of volcanic unrest requires knowledge of the architecture of the magmatic system, particularly the depths at which magmas are stored. Such information can also be vital to help predict changes in eruptive style and vigour. However, popular petrological tools to assess magma storage depths (e.g., melt inclusions - MI) are costly, uncertainty-ridden, and too slow for real-time monitoring. Here, we evaluate the reliability and efficiency of Raman Spectroscopy measurements of CO₂-dominated fluid inclusions (FI) as a rapid geobarometer relative to more established methods such as microthermometry and MI barometry. We calculate storage pressures for 130 olivine-hosted FI from the 2018 Lower East Rift Zone eruption of Kīlauea, which are statistically indistinguishable to those determined from MI. We show that calibrated Raman spectroscopy yields densities within 5-10% of microthermometry measurements for CO₂-dominated FI but is a far more suitable method for systems like Kīlauea dominated by shallow magma storage. Overall, pressures determined from FI by Raman spectroscopy are robust, and require only a fraction of the work, time, and resources, with potential for near real-time monitoring.

Keywords Fluid inclusions · CO₂ · Raman spectroscopy · geobarometry · Kīlauea volcano

1 Introduction

Determining the depths of magma storage is essential to interpreting signals of volcanic unrest and to help predict changes in eruptive style and vigour. Magma storage depth is commonly determined using erupted materials and petrological tools like melt inclusion (MI), mineral-mineral and mineral-melt barometry (Klügel et al., 2005; Putirka, 2008; Barker et al., 2021). However, many petrological tools are uncertainty-ridden (i.e., ±8-19 km clinopyroxene-based barometers, Wieser et al. (2023)), and/or too slow to make them suitable for real-time monitoring. For example, MI work involves numerous time and resource consuming sample preparation, analytical, and data processing steps (Fig. 1a). Even after such meticulous work, calculated pressures are typically associated with considerable analytical and systematic uncertainties (e.g., melt and bubble volume measurements, solubility models, post-entrapment crystallization corrections), ranging from 20% to 50% when fully propagated (Tucker et al., 2019; Wieser et al., 2021; DeVitre et al., 2023).

CO₂-rich fluid inclusions (FI), tiny droplets of exsolved fluids trapped in crystals as they grow from a melt (Roedder, 1979), provide an intriguing alternative to MI when the main goal is to deduce magma storage depths. The density of CO₂ in FI is a strong function of pressure, with little sensitivity to temperature (Dayton et al., 2023). Thus, if density is well-constrained, and a reasonable estimate is made of entrapment temperature, the entrapment pressure can be directly calculated through an equation of state (Fig. 1c). Conventionally, CO₂ densities have been determined by microthermometry through observation of phase changes during heating and cooling – this method has been successfully applied to CO₂-rich volcanic systems characterized by deep magma storage systems such as the Canary Islands, Cabo Verde Islands, and the Azores (Klügel et al., 2005; Klügel et al., 2020; Zanon & Frezzotti, 2013). However, it is difficult to measure FI trapped in shallower volcanic systems (< 6 km) by microthermometry, because the density of CO₂ is

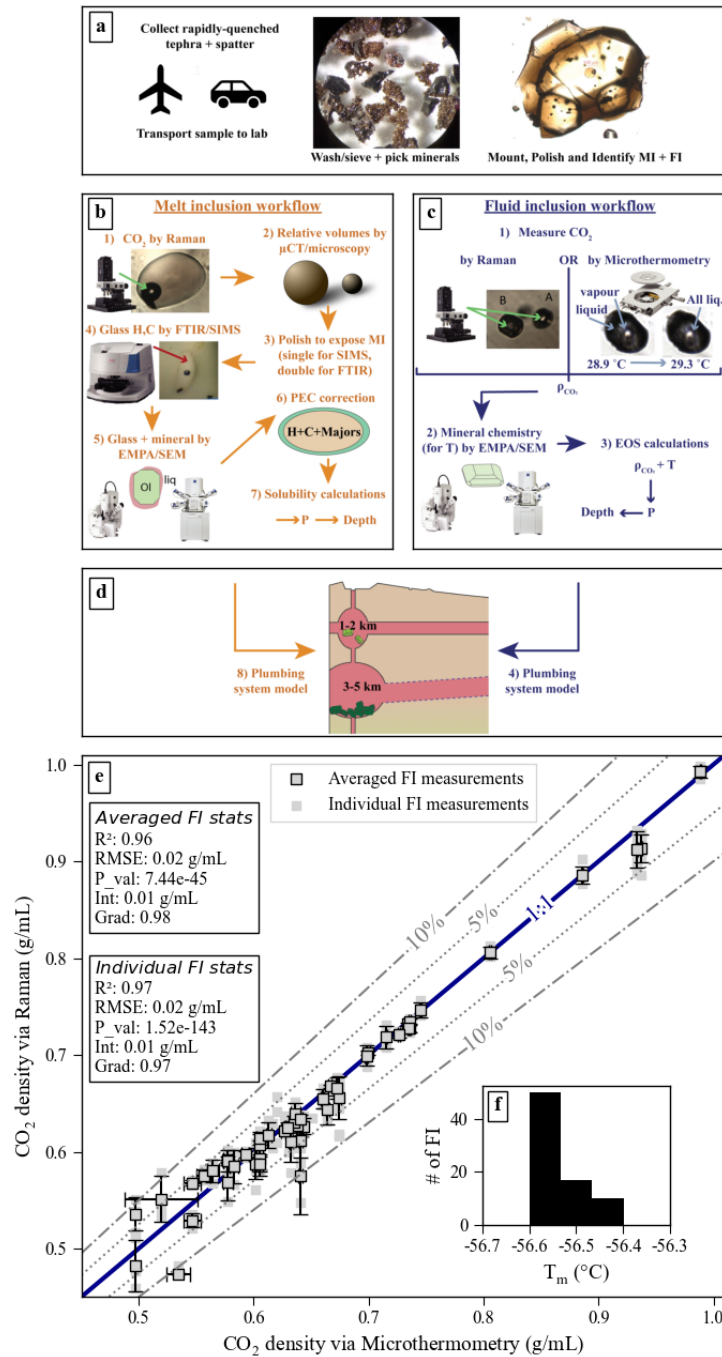


Figure 1: MI and FI workflows for magma storage depths measurements and comparison of CO₂ densities obtained by micro thermometry to those obtained via calibrated Raman Spectroscopy for the same FI. (a) Common steps in MI and FI workflows (b) MI workflow (c) FI workflow to deduce the geometry of the plumbing system (d). (e) Density via Raman vs density obtained from micro thermometry. Outlined symbols represent averaged Raman measurement for each FI, no-outline symbols are individual Raman measurements. Error bars show $\pm 1\sigma$ of repeated measurements for Raman and microthermometry.

below critical, and the homogenization of the liquid into the vapor phase is nearly impossible to observe (Hansteen & Klügel, 2008). Microthermometry also requires the use of specialized heating/cooling stages, the preparation of doubly polished crystal wafers (Fig. 1c) and is limited by the ability to optically observe phase changes. The past decade of advances in the accuracy and precision of Raman-based CO₂ densimetry has opened new avenues for the technique. This means that low bulk CO₂ density (<0.45 g/mL) and very small FI (down to 1 μm), which are impossible to measure by microthermometry, can be measured by Raman with an accuracy generally better than 0.02 g/mL (Yuan & Mayanovic, 2017). Raman analyses also only require a single polish to ensure visibility of the FI within 50 μm of the surface, resulting in fewer preparation steps than necessary for both microthermometry and MI workflows (Fig. 1a-d). Raman is also a more accessible method as it is commonly used in fields like material science and physics and is therefore widely available in research institutions. Recent work also indicates that FI may have potential as a real-time petrological monitoring tool as they can be used to relatively rapidly constrain the depth of magma storage (Dayton et al., 2023).

Nevertheless, FI are often prone to a variety of post-entrapment modifications, such as stretching and decrepitation and may be subject to significant re-equilibration prior to eruption (e.g., Wanamaker & Evans (1989) and Hansteen & Klügel (2008)). Re-equilibration is often thought to be rapid, such that FI may reflect stalling levels rather than true capture depths (Hansteen & Klügel, 2008; Zanon & Frezzotti, 2013), or even be reset during slow quenching (Klügel et al., 2020). This brings us to an essential question as Raman-based FI barometry grows in popularity: are the storage depths estimated using CO₂-dominated FI consistent with those constrained by MI barometry and other estimates of magma storage depths or are they always reset by late-stage processes as magmas ascend to the surface?

The 2018 Lower East Rift Zone (LERZ) eruption of Kīlauea volcano in Hawai'i is an ideal test bed to assess FI barometry, given that this volcano is extremely well monitored, and geophysical methods have revealed two main regions of magma storage (1-2 km depth, and 3-5 km, Baker & Amelung (2012), Anderson & Poland (2016), and Anderson et al. (2019)). These geophysical estimates were corroborated by MI work on erupted 2018 samples (Lerner et al., 2021; Wieser et al., 2021). However, it is notable that both MI studies were submitted 2 years after the eruption had ended, a testament of the considerable analytical effort required (Fig. 1a-d), and thus the unsuitability of this method as a monitoring tool. Here, we assess whether magma storage depths determined using Raman analyses of CO₂-dominated FI would have yielded the same results. First, we assess the accuracy of the Raman method through a direct comparison with microthermometry. Then, we compare pressures from 130 FI hosted in olivine crystals to MI pressures from the exact same samples (and sometimes even the same crystals). Our results show that magma storage depths calculated from FI barometry and MI barometry are statistically indistinguishable, yet FI have significantly smaller uncertainties, and require far fewer preparation and analytical steps (Fig. 1c vs 1b).

2 Calibrated Raman spectroscopy is a suitable alternative to microthermometry.

Despite its relative ease compared with microthermometry (Fig. 1c), and ability to assess a wider range of CO₂ densities, many aspects of the Raman method have been recently criticized (e.g., peak fitting, instrument drift, instrument calibrations), with suggestions it is '150X less accurate than microthermometry' (Bakker, 2021). To assess whether Raman spectroscopy can reliably be used to measure the density of CO₂-dominated FI, we measured olivine-hosted FI from Fogo volcano using both our calibrated Raman instrument and microthermometry ($\rho_{\text{CO}_2} > 0.45$ g/mL; Fig. 1d; Fig. S-1 in SI Methods).

Melting temperatures for all FI analysed using microthermometry (11 crystals, 60 FI) are 56.5 ± 0.1 °C (Fig. 1e) which precludes the presence of any gaseous species other than CO₂ (confirmed via Raman Spectroscopy). Homogenization temperatures obtained range from -11.1 ± 0.1 to 31.6 ± 1 °C (Fig. S-1b) and yield calculated bulk densities between 0.49 and 0.99 g/mL (Fig. 1e). Results of microthermometry and calibrated Raman spectroscopy are generally within 5% of each other (Fig. 1d), and up to 10% for inclusions with near-critical CO₂ densities (~0.45 g/mL), where microthermometry become extremely sensitive to the accuracy of the homogenization temperature (Hansteen & Klügel, 2008). Regression statistics confirms good agreement between the two methods ($R^2=0.96$, RMSE=0.02 g/mL, p-val<0.000). Overall, this comparison validates Raman spectroscopy measurements as a suitable alternative to microthermometric measurements (see also Kobayashi et al. (2012)).

3 Texturally related FI and MI in same crystals record the same entrapment pressures.

Now that we have validated the Raman method to measure CO₂ densities, we wish to test whether FI pressures are a suitable alternative to the more widely used MI method. The most robust comparison examines pressures from MI and FI within a single crystal. Therefore, we identify and measure 32 CO₂-rich FI in 17 crystals containing MIs measured by Wieser et al. (2021) (Fig. 2). Petrographic work was done to categorized FI depending on their shapes, position, and textural relationship to the MI. Fig. 2a shows a crystal with 4 FI in a similar textural environment to the measured MI; pressure overlap within uncertainty (Fig. 2b). Overall, we find that FI hosted in the same crystals, same inclusion

assemblages or apparent growth zones record the same entrapment pressures as reconstructed MI within the uncertainty of the methods (Fig. 2c). The large error on melt inclusions pressures is notable during these comparisons, largely resulting from uncertainty in the relative volume of the vapour bubble (Wieser et al., 2021; Tucker et al., 2019; DeVitre et al., 2023). The uncertainty on FI pressures (see supporting info) is much smaller, resulting from the propagation of errors from peak fitting, instrument drift, the densimeter, and the entrapment temperature (Wieser & DeVitre, 2023).

In contrast, Fig. 2d shows texturally-unrelated FI and MI – the FI is present in the same crystal cluster but within a separate smaller crystal. If crystals were attached via synneusis (Wieser et al., 2019; DiBenedetto et al., 2020), it is very plausible the smaller crystal grew in a different environment, explaining the lower FI pressure (Fig. 2e). In general, it appears that if FI are well documented and selected with care (i.e., FI in crystal core growth zones), the estimates of pressure for FI are consistent with those from MI work at Kīlauea.

4 FI and MI pressures yield a consistent petrogenetic model.

Due to the scarcity of FI in the exact same crystal as MI, direct comparisons are limited. To complement our dataset, we also analysed additional 100 FI in olivine crystals picked directly from the same sample split as the MI. We remove FI with a significant melt film (>20% vol, see supporting information), leaving 102 FI to compare with 103 MI from Wieser et al. (2021). When subdivided by sample (May, July, Aug 2018), histograms indicate good agreement between the pressures recorded by FI and MI (Fig. 3 a-c), particularly when considering the analytical uncertainty associated with MI measurements containing a vapour bubble (orange MI w/VB error bar).

We apply the Kolmogorov–Smirnov test (KS) to assess whether slight visual differences are statistically significant. Sample KS tests indicate that MI and FI pressures are not significantly different for May and August 2018 (p-val = 0.09 and 0.06 respectively) but suggest a possible significant difference for July 2018 (p-val=0.001). However, such comparisons are restricted by the relatively small N for each sample (N<50), and the relatively large analytical errors on MI measurements. To address this, we apply a Monte-Carlo simulation using Python3 to resample each MI and FI measurement 1000 times within analytical uncertainty. KS tests applied to these resampled distributions indicate that the FI and MI pressure distributions are not significantly different for any of the 3 events (p-val = 0.39±0.20, 0.04±0.04 and 0.05±0.07 for May, July and August respectively) and differences can be explained by the uncertainty in the MI measurements.

So far, we have only considered the analytical uncertainty associated with MI and FI saturation pressures. However, reconstructed MI H₂O and CO₂ concentrations are converted into pressures using a solubility model, which introduces a large amount of systematic uncertainty. On Fig. 3g-i, we show pressures calculated using the MagmaSat model (Ghiorso & Gualda, 2015), which Wieser et al. (2021) suggest is the most suitably calibrated model at Kīlauea. However, this is little consensus; for the same eruption, Lerner et al. (2021) use the solubility model of Iacono-Marziano et al. (2012). To demonstrate the magnitude of this uncertainty, we show cumulative MI pressures for 5 different solubility models (Newman & Lowenstern, 2002; Iacono-Marziano et al., 2012; Shishkina et al., 2014; Allison et al., 2022; Ghiorso & Gualda, 2015). Clearly, the uncertainty related to model choice can easily account for any slight differences between MI and FI pressures. Another advantage of FI barometry compared to MI barometry is that the choice of EOS does not significantly contribute to the uncertainty (Hansteen & Klügel, 2008).

Slight differences between FI and MI pressures could also be explained through sampling bias relating to the complex histories of the 2018 crystal cargo. Wieser et al. (2021) and Lerner et al. (2021) suggest that crystals are derived from two storage reservoirs beneath Kīlauea's summit based on the relationship between MI Saturation pressures and olivine Fo content. FI pressures confirm this relationship – those trapped in lower Fo content olivine crystals tend to have lower pressures of entrapment (Fig 4). This demonstrates that similar petrogenetic interpretations can be made with both FI and MI.

5 Assessing FI re-equilibration

While differences between MI and FI are not statistically significant and are easily overwhelmed by the uncertainty in volatile solubility models, some FIs do appear to record shallower pressures than MI for an equivalent olivine Fo content. While MI suffer from systematic uncertainties relating to solubility models (Fig. 3d-f), the main source of systematic uncertainty affecting FI is the process of re-equilibration during prolonged storage and transport. To assess whether re-equilibration could explain the seemingly lower pressures recorded by FI in July 2018, we constructed a Python3 implementation of the mechanical re-equilibration model of Wanamaker & Evans (1989) based on olivine relaxation through dislocation creep (SI notebook). We model the effect of FI stretching on the internal pressure and CO₂ density for FI using the EOS of Span & Wagner (1996). We consider FI with a radius of 1 and 20 μm at variable distances (50-500 μm) from crystal defect structures (i.e., cracks, crystal edges and boundaries). First, we consider FI which may have been trapped in the deeper South Caldera reservoir (4 km, 1300 °C) before being mobilized to the Halema'uma'u reservoir (1 km depth, 1150 °C), and stored for 0-2 years prior to eruption (based on diffusion

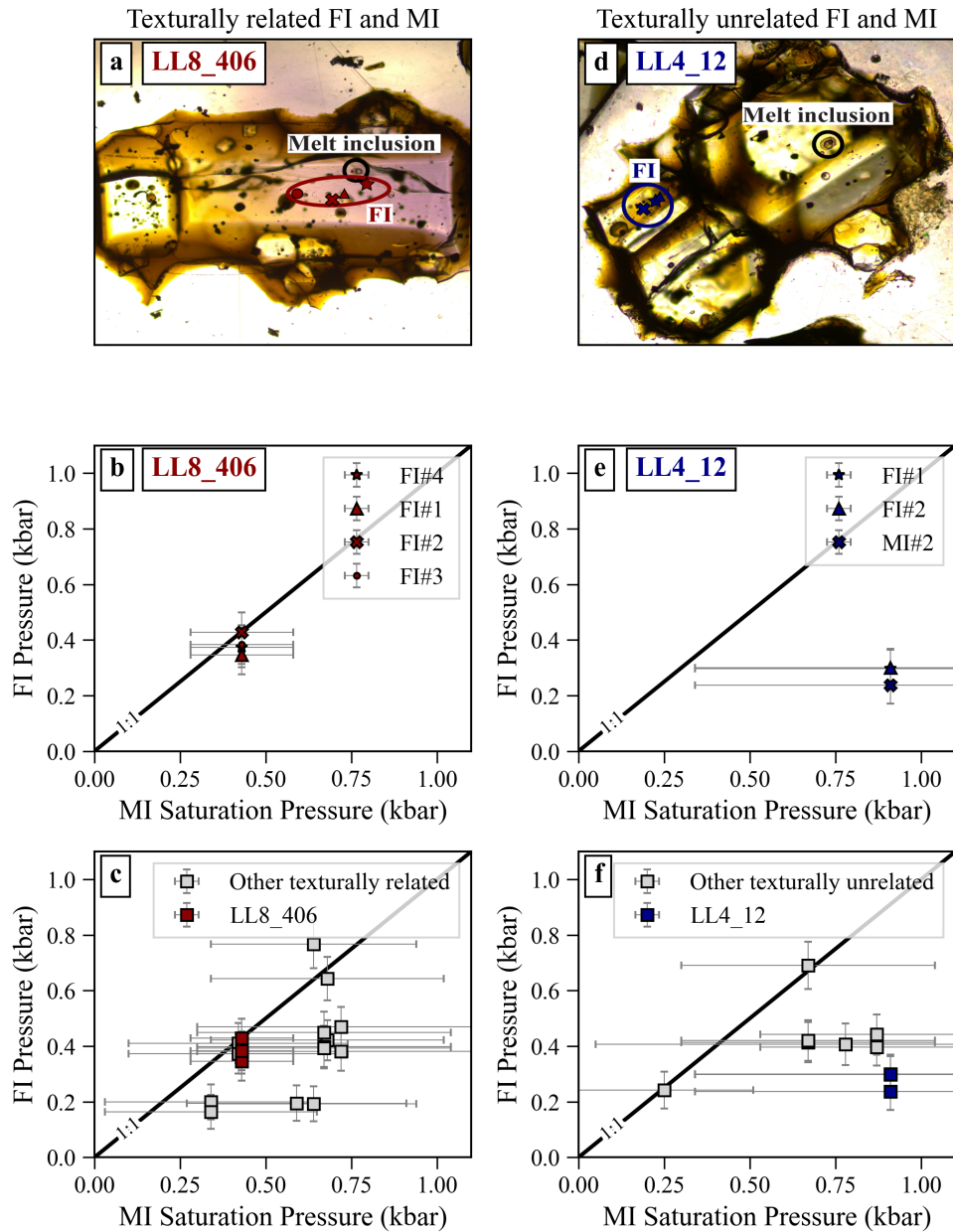


Figure 2: FI vs MI in the same crystal and/or crystal clusters. The left side shows texturally related FI and MI, the right side shows texturally unrelated FI and MI (a) Crystal with texturally related MI and FI (LL8_406) showing overlapping pressures (b). (c) Grey squares show other texturally related MI and FI. (d) Crystal with texturally-unrelated MI and FI (LL4_12)– FI are found in a smaller olivine crystal in the same crystal cluster and return lower pressures (e). (f) grey squares show other texturally unrelated FI and MI.

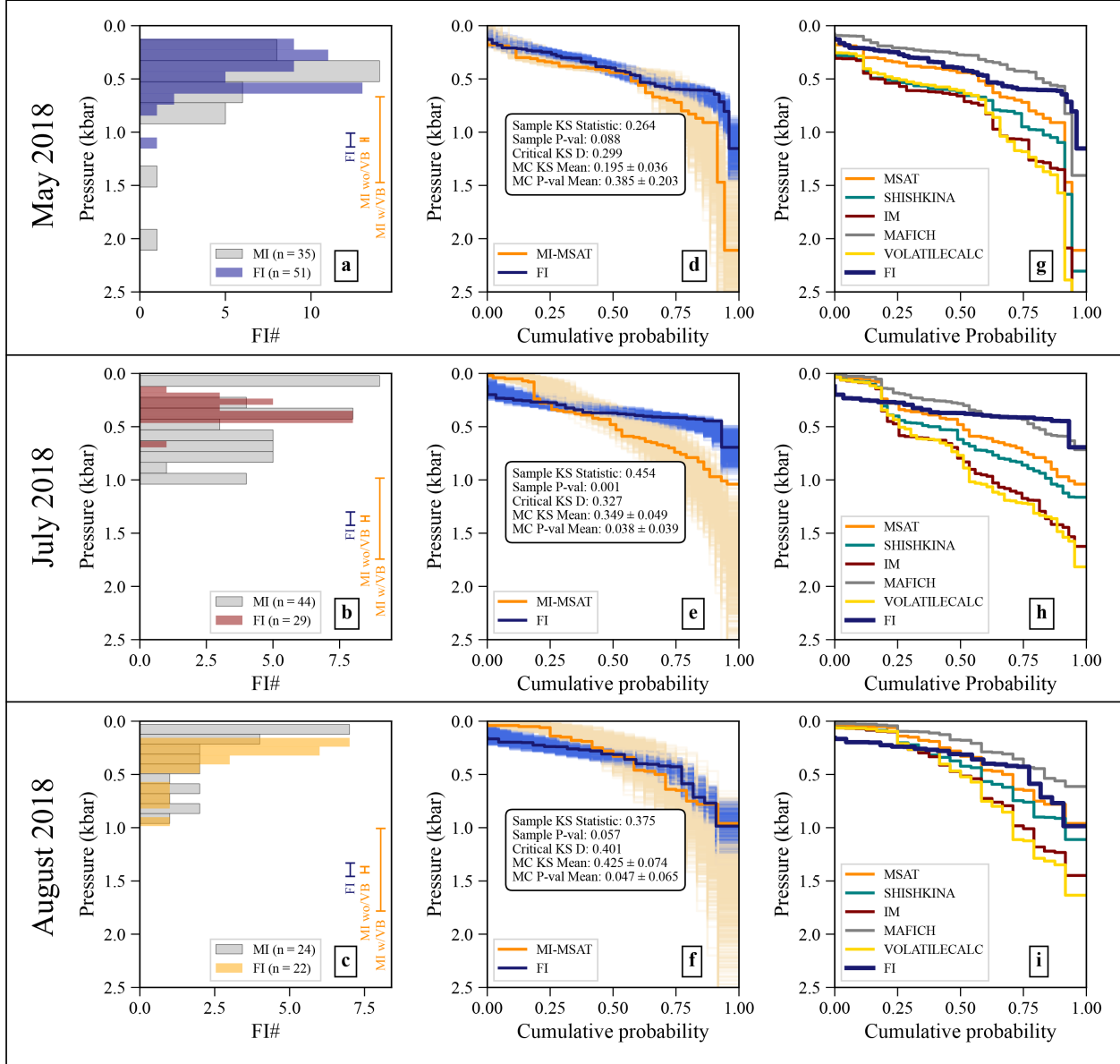


Figure 3: Comparing FI and MI pressures for May, July and August 2018. a-c) Histograms of pressures, with error bars indicate the average 1σ uncertainty for MI with vapor bubbles (MI w/VB) and without vapor bubbles (MI wo/VB), and the average 1σ FI uncertainty. (d-f) Results of KS tests comparing FI and MI pressure cumulative probability functions (CDF) from Monte-Carlo simulations. For MI, the MagmaSat results are shown. (g-i) Pressure CDF for analysed FI and MI using 5 different solubility models: MagmaSat (MSAT), Shishkina (SHISHKINA), Iacono-Marziano (IM), Mafich (MAFICH), VolatileCalc (VOLATILECALC) (Newman & Lowenstern, 2002; Iacono-Marziano et al., 2012; Shishkina et al., 2014; Allison et al., 2022; Ghiroso & Gualda, 2015)

timescales from Mourey et al. (2023), Fig. 4e). In the most extreme case (stretching of a 20 μm radius FI found 50 μm from a crystal defect), stalling for 2 years causes a decrease in CO₂ density of less than 10%, which is smaller than the average measurement uncertainty.

It has also been suggested that FI erupted in lava flows may re-equilibrate as the host crystal cools at atmospheric pressure (Klügel et al., 2020). The May-18 sample is a rapidly quenched reticulite, and the Aug-18 sample was water-quenched from the lava channel. In contrast, the July-18 sample was an air-cooled overflow from the channel. Based on observing other overflows, we predict that cooling occurred within hours. However, even allowing up to 7 days re-equilibration results in less than 1% difference (Fig. 4f), well within analytical uncertainty. Overall, our results

indicate that in shallow systems such as that of Kīlauea where the internal pressure of the FI is relatively low, stretching on timescales relevant to magma storage, eruption and quenching is unlikely to play a major role and re-equilibration is of no significant concern. Therefore, we conclude that Raman-based measurements of FI can be used to constrain the storage depths of magmas in CO₂-dominated shallow volcanic systems.

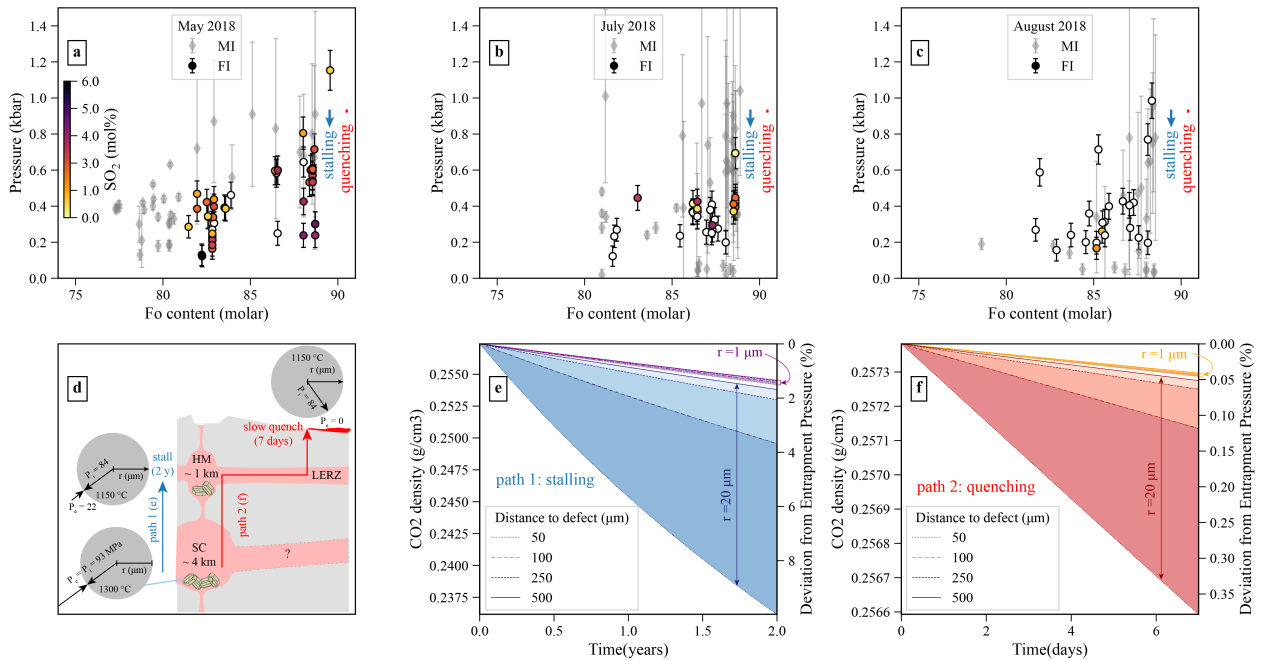


Figure 4: Assessing crystal cargoes and FI re-equilibration. (a-c) MI and FI pressures vs Fo content of the host olivine for (a) May 2018 (b) July 2018 (c) August 2018. FI are coloured by calculated SO₂ (mol%) based on the method of Burke (2001). (d) Schematic diagram of Kīlauea plumbing system showing the scenarios modelled in e and f. (e) Stretching model for stalling scenario (d) for 1 and 20 μm radii FI captured at SC reservoir. (f) Stretching model for slow-quenching scenario (d). Arrows depicting the worst-case scenario from each model are shown in a-c.

6 Conclusions

Here, we compare barometric estimates of magma storage depths for the 2018 LERZ eruption of Kīlauea volcano using CO₂-dominated FI to those obtained via MI studies. We find that FI captured at Kīlauea are unlikely to be significantly affected by re-equilibration on timescales relevant to magma storage and migration. Within uncertainty, they reflect the same entrapment depths as those recorded by MI in the same sample splits. Therefore, FI are a suitable alternative to MI for barometry in shallow CO₂-rich volcanic systems.

7 Author contributions

CLJD prepared the Fogo FI, performed all Raman and Microthermometry analyses, developed the MC subsampling and FI re-equilibration code, and wrote the manuscript. PW acquired the funding, prepared the Kīlauea FI, wrote the peak fitting/EOS code, and edited the manuscript.

8 Acknowledgements

PW and CLJD acknowledge support from NSF EAR 2217371 and the Berkeley Rose Hills Innovator Program. We thank Ricardo S. Ramalho for collecting the Fogo volcano samples. This work was possible thanks to the fabulous samples collected by USGS field teams in 2018 and particularly Frank Trusdell for helping with lava sampling as part of the PlumeTeam 2018 aerosol campaign.

9 Data availability

All data are made available with the publication. All data are also available on Github (<https://github.com/cljdevitre/KilaueaMIFI2023>) along with notebooks to reproduce figures published in the article, the notebooks for running the MC KS test simulations and data processing notebooks for DiadFit. The Github repo will be archived at Zenodo upon article acceptance. Documentation for the python3 tool (<https://github.com/cljdevitre/RelaxiFI>) developed to assess re-equilibration of FI is available at <https://relaxifi.readthedocs.io/>.

References

- Allison, Chelsea M.; Roggensack, Kurt & Clarke, Amanda B. (Mar. 19, 2022). *MafiCH: a general model for H₂O–CO₂ solubility in mafic magmas*. In: *Contributions to Mineralogy and Petrology* 177.3, 40. ISSN: 1432-0967. DOI: 10.1007/s00410-022-01903-y. URL: <https://doi.org/10.1007/s00410-022-01903-y> (visited on 05/13/2022).
- Anderson, Kyle R. & Poland, Michael P. (Aug. 1, 2016). *Bayesian estimation of magma supply, storage, and eruption rates using a multiphysical volcano model: Kīlauea Volcano, 2000–2012*. In: *Earth and Planetary Science Letters* 447, 161–171. ISSN: 0012-821X. DOI: 10.1016/j.epsl.2016.04.029. URL: <https://www.sciencedirect.com/science/article/pii/S0012821X16302011> (visited on 09/19/2023).
- Anderson, Kyle R. et al. (Dec. 6, 2019). *Magma reservoir failure and the onset of caldera collapse at Kīlauea Volcano in 2018*. In: *Science* 366.6470. Publisher: American Association for the Advancement of Science, eaaz1822. DOI: 10.1126/science.aaz1822. URL: <https://www.science.org/doi/10.1126/science.aaz1822> (visited on 09/19/2023).
- Baker, Scott & Amelung, Falk (2012). *Top-down inflation and deflation at the summit of Kīlauea Volcano, Hawai'i observed with InSAR*. In: *Journal of Geophysical Research: Solid Earth* 117 (B12). _eprint: <https://onlinelibrary.wiley.com/doi/pdf/10.1029/2011JB009123>. ISSN: 2156-2202. DOI: 10.1029/2011JB009123. URL: <https://onlinelibrary.wiley.com/doi/abs/10.1029/2011JB009123> (visited on 09/19/2023).
- Bakker, Ronald J. (2021). *The perfection of Raman spectroscopic gas densimeters*. In: *Journal of Raman Spectroscopy* 52.11. _eprint: <https://onlinelibrary.wiley.com/doi/pdf/10.1002/jrs.6245>, 1923–1948. ISSN: 1097-4555. DOI: 10.1002/jrs.6245. URL: <https://onlinelibrary.wiley.com/doi/abs/10.1002/jrs.6245> (visited on 09/13/2023).
- Barker, Abigail K.; Rydeblad, Elin M. & Silva, Sónia M. D. M. (2021). “Magma Storage at Ocean Islands”. In: *Crustal Magmatic System Evolution*. Section: 3 _eprint: <https://onlinelibrary.wiley.com/doi/pdf/10.1002/9781119564485.ch3>. American Geophysical Union (AGU), 45–78. ISBN: 978-1-119-56448-5. DOI: 10.1002/9781119564485.ch3. URL: <https://onlinelibrary.wiley.com/doi/abs/10.1002/9781119564485.ch3> (visited on 07/26/2022).
- Burke, Ernst A. J. (Jan. 1, 2001). *Raman microspectrometry of fluid inclusions*. In: *Lithos. Fluid Inclusions: Phase Relationships - Methods - Applications*. A Special Issue in honour of Jacques Touret 55.1, 139–158. ISSN: 0024-4937. DOI: 10.1016/S0024-4937(00)00043-8. URL: <https://www.sciencedirect.com/science/article/pii/S0024493700000438> (visited on 09/19/2023).
- Dayton, Kyle et al. (Feb. 8, 2023). *Deep magma storage during the 2021 La Palma eruption*. In: *Science Advances* 9.6. Publisher: American Association for the Advancement of Science, eade7641. DOI: 10.1126/sciadv.ade7641. URL: <https://www.science.org/doi/full/10.1126/sciadv.ade7641> (visited on 04/25/2023).
- DeVitre, Charlotte L. et al. (Aug. 15, 2023). *Oceanic intraplate explosive eruptions fed directly from the mantle*. In: *Proceedings of the National Academy of Sciences* 120.33. Publisher: Proceedings of the National Academy of Sciences, e2302093120. DOI: 10.1073/pnas.2302093120. URL: <https://www.pnas.org/doi/10.1073/pnas.2302093120> (visited on 08/15/2023).
- DiBenedetto, Michelle; Qin, Zhipeng & Suckale, Jenny (Dec. 4, 2020). *Crystal aggregates record the pre-eruptive flow field in the volcanic conduit at Kīlauea, Hawaii*. In: *Science Advances* 6.49. Publisher: American Association for the Advancement of Science, eabd4850. DOI: 10.1126/sciadv.abd4850. URL: <https://www.science.org/doi/10.1126/sciadv.abd4850> (visited on 09/13/2023).
- Ghiorso, Mark S. & Gualda, Guilherme A. R. (June 5, 2015). *An H₂O–CO₂ mixed fluid saturation model compatible with rhyolite-MELTS*. In: *Contributions to Mineralogy and Petrology* 169.6, 53. ISSN: 1432-0967. DOI: 10.1007/s00410-015-1141-8. URL: <https://doi.org/10.1007/s00410-015-1141-8> (visited on 05/13/2022).
- Hansteen, Thor H. & Klügel, Andreas (Jan. 1, 2008). *Fluid Inclusion Thermobarometry as a Tracer for Magmatic Processes*. In: *Reviews in Mineralogy and Geochemistry* 69.1, 143–177. ISSN: 1529-6466. DOI: 10.2138/rmg.2008.69.5. URL: <https://doi.org/10.2138/rmg.2008.69.5> (visited on 08/28/2023).
- Iacono-Marziano, Giada et al. (2012). *New experimental data and semi-empirical parameterization of H₂O–CO₂ solubility in mafic melts*. In: *Geochimica et Cosmochimica Acta* 97. ISBN: 0016-7037 Publisher: Elsevier, 1–23.

- Klügel, Andreas; Hansteen, Thor H. & Galipp, Karsten (July 30, 2005). *Magma storage and underplating beneath Cumbre Vieja volcano, La Palma (Canary Islands)*. In: *Earth and Planetary Science Letters* 236.1, 211–226. ISSN: 0012-821X. DOI: 10.1016/j.epsl.2005.04.006. URL: <https://www.sciencedirect.com/science/article/pii/S0012821X05002141> (visited on 08/28/2023).
- Klügel, Andreas et al. (2020). *Magma Plumbing During the 2014–2015 Eruption of Fogo (Cape Verde Islands)*. In: *Frontiers in Earth Science* 8. ISSN: 2296-6463. URL: <https://www.frontiersin.org/articles/10.3389/feart.2020.00157> (visited on 07/27/2022).
- Kobayashi, Tomoyuki et al. (2012). *Conformity and precision of CO₂ densimetry in CO₂ inclusions: microthermometry versus Raman microspectroscopic densimetry*. In: *Journal of Raman Spectroscopy* 43.8. _eprint: <https://onlinelibrary.wiley.com/doi/pdf/10.1002/jrs.3134>, 1126–1133. ISSN: 1097-4555. DOI: 10.1002/jrs.3134. URL: <https://onlinelibrary.wiley.com/doi/abs/10.1002/jrs.3134> (visited on 09/13/2023).
- Lerner, Allan H. et al. (2021). *The petrologic and degassing behavior of sulfur and other magmatic volatiles from the 2018 eruption of Kīlauea, Hawai'i: melt concentrations, magma storage depths, and magma recycling*. In: *Bulletin of Volcanology* 83.6. ISBN: 1432-0819 Publisher: Springer, 1–32.
- Mourey, Adrien J. et al. (Feb. 28, 2023). *Years of magma intrusion primed Kīlauea Volcano (Hawai'i) for the 2018 eruption: evidence from olivine diffusion chronometry and monitoring data*. In: *Bulletin of Volcanology* 85.3, 18. ISSN: 1432-0819. DOI: 10.1007/s00445-023-01633-4. URL: <https://doi.org/10.1007/s00445-023-01633-4> (visited on 09/13/2023).
- Newman, Sally & Lowenstern, Jacob B. (June 1, 2002). *VolatileCalc: a silicate melt–H₂O–CO₂ solution model written in Visual Basic for excel*. In: *Computers & Geosciences* 28.5, 597–604. ISSN: 0098-3004. DOI: 10.1016/S0098-3004(01)00081-4. URL: <https://www.sciencedirect.com/science/article/pii/S0098300401000814> (visited on 12/10/2022).
- Putirka, Keith D. (2008). *Thermometers and barometers for volcanic systems*. In: *Reviews in mineralogy and geochemistry* 69.1. ISBN: 1529-6466 Publisher: Mineralogical Society of America, 61–120.
- Roedder, Edwin (1979). *Origin and significance of magmatic inclusions*. In: *Bulletin de Minéralogie* 102.5. Publisher: Persée - Portail des revues scientifiques en SHS, 487–510. DOI: 10.3406/bulmi.1979.7299. URL: https://www.persee.fr/doc/bulmi_0180-9210_1979_act_102_5_7299 (visited on 07/26/2022).
- Shishkina, Tatiana A. et al. (Nov. 21, 2014). *Compositional and pressure effects on the solubility of H₂O and CO₂ in mafic melts*. In: *Chemical Geology* 388, 112–129. ISSN: 0009-2541. DOI: 10.1016/j.chemgeo.2014.09.001. URL: <https://www.sciencedirect.com/science/article/pii/S000925411400415X> (visited on 07/29/2022).
- Span, Roland & Wagner, Wolfgang (1996). *A new equation of state for carbon dioxide covering the fluid region from the triple-point temperature to 1100 K at pressures up to 800 MPa*. In: *Journal of physical and chemical reference data* 25.6. ISBN: 0047-2689 Publisher: American Institute of Physics for the National Institute of Standards and ... , 1509–1596.
- Tucker, Jonathan M. et al. (2019). *A high carbon content of the Hawaiian mantle from olivine-hosted melt inclusions*. In: *Geochimica et Cosmochimica Acta* 254. ISBN: 0016-7037 Publisher: Elsevier, 156–172.
- Wanamaker, B. J. & Evans, Brian (Mar. 1, 1989). *Mechanical re-equilibration of fluid inclusions in San Carlos olivine by power-law creep*. In: *Contributions to Mineralogy and Petrology* 102.1, 102–111. ISSN: 1432-0967. DOI: 10.1007/BF01160194. URL: <https://doi.org/10.1007/BF01160194> (visited on 08/20/2023).
- Wieser, P. E. et al. (2021). *Reconstructing Magma Storage Depths for the 2018 Kīlauean Eruption From Melt Inclusion CO₂ Contents: The Importance of Vapor Bubbles*. In: *Geochemistry, Geophysics, Geosystems* 22.2. _eprint: <https://onlinelibrary.wiley.com/doi/pdf/10.1029/2020GC009364>, e2020GC009364. ISSN: 1525-2027. DOI: 10.1029/2020GC009364. URL: <https://onlinelibrary.wiley.com/doi/abs/10.1029/2020GC009364> (visited on 07/28/2022).
- Wieser, Penny E et al. (Feb. 1, 2023). *Barometers Behaving Badly I: Assessing the Influence of Analytical and Experimental Uncertainty on Clinopyroxene Thermobarometry Calculations at Crustal Conditions*. In: *Journal of Petrology* 64.2, egac126. ISSN: 0022-3530. DOI: 10.1093/petrology/egac126. URL: <https://doi.org/10.1093/petrology/egac126> (visited on 09/19/2023).
- Wieser, Penny E. & DeVitre, Charlotte L. (Apr. 4, 2023). *DiadFit: An Open-SourcePython3 Tool for Peak fitting of Raman Data from silicate melts and CO₂ fluids*. In: Publisher: EarthArXiv. URL: <https://eartharxiv.org/repository/view/5236/> (visited on 08/20/2023).
- Wieser, Penny E. et al. (Aug. 20, 2019). *To sink, swim, twin, or nucleate: A critical appraisal of crystal aggregation processes*. In: *Geology* 47.10, 948–952. ISSN: 0091-7613. DOI: 10.1130/G46660.1. URL: <https://doi.org/10.1130/G46660.1> (visited on 09/13/2023).
- Yuan, Xueyin & Mayanovic, Robert A. (Oct. 1, 2017). *An Empirical Study on Raman Peak Fitting and Its Application to Raman Quantitative Research*. In: *Applied Spectroscopy* 71.10. Publisher: Society for Applied Spectroscopy, 2325–2338. URL: <https://opg.optica.org/as/abstract.cfm?uri=as-71-10-2325> (visited on 05/13/2022).
- Zanon, Vittorio & Frezzotti, Maria Luce (2013). *Magma storage and ascent conditions beneath Pico and Faial islands (Azores archipelago): A study on fluid inclusions*. In: *Geochemistry, Geophysics, Geosystems* 14.9. _eprint:

<https://onlinelibrary.wiley.com/doi/pdf/10.1002/ggge.20221>, 3494–3514. ISSN: 1525-2027. DOI: 10.1002/ggge.20221. URL: <https://onlinelibrary.wiley.com/doi/abs/10.1002/ggge.20221> (visited on 08/28/2023).

Reliability of Raman analyses of CO₂-rich fluid inclusions as a rapid barometer at Kīlauea

Charlotte L. DeVitre, Penny E. Wieser

Supplementary Information

The Supplementary Information includes:

- 1. Detailed materials and methods
- 2. Statistical significance of the MI vs FI recorded pressures
- 3. Fluid % effect on calculated densities and pressures
- Figures S-1 to S-6. Figures are included in the text where relevant.
- Data Table S-1 (on Github)
- Image Database S-1 (on Github)
- Dataset S-1 (Collection of spectra, Jupyter Lab notebooks to process and plot data, on Github).
- Supplementary Information References

1. Detailed materials and methods

1.1 Samples

Olivines from three samples of the 2018 LERZ eruption of Kīlauea volcano in Hawai'i (Fissure 8 samples of May, July and August 2018) were picked under a binocular microscope, and individually mounted in CrystalBond™ on glass slides from jaw crushed and sieved samples as described in (Wieser *et al.*, 2021). The May 2018 sample erupted on May 30, 2018 (Lab code LL4, USGS code KE62–3293), as vesicular reticulite and scoria; The July 2018 sample erupted in mid-July, 2018 (Lab code LL8, no USGS code) was sampled from the selvages of a naturally quenched, and highly vesicular proximal overflow from the Fissure 8 channel; The August 2018 sample erupted on August 1st, 2018 (Lab code LL7, USGS code KE62–A3321F) and was sampled directly from the channel and rapidly quenched in water (Wieser *et al.*, 2021). FI were revealed by grinding using 250–3,000 grade wet and dry paper. Petrographic work was done to describe the emplacement of FI and FIA in the crystals. Photos were taken of the crystals and FI (see Image Database S-1). Additionally, FI were located and photographed in the same crystals as those in which melt inclusions were analyzed in (Wieser *et al.*, 2021). In total we analyzed 146 FI hosted in 57 olivine crystals 2018 LERZ eruption of Kīlauea volcano.

Olivines from tephra of the 1951 eruption of Fogo Volcano in Cabo Verde (DeVitre *et al.*, 2023), were also picked under binocular microscope and individually mounted in CrystalBond™. FI were revealed by grinding using 600-2000 grit wet paper and polish refined using 1 and 0.3 um wet paper and alumina paste. These crystals were doubly polished for micro thermometric analyses. We analyzed 63 FI in 12 crystals of this eruption in one week.

1.2 Raman spectroscopy FI CO₂

We collected Raman spectra using a WiTec Alpha 300R Raman spectrometer at the Department of Earth and Planetary Sciences at the University of California, Berkeley. We use a green solid state 532.046 nm laser focused as an excitation source with a 50x objective (x0.55NA, 9.1 mm focal distance) and 100x objective (x0.95NA, 4mm WD). The system is equipped with TruePower system which allows for in-fiber power adjustments of <0.1 mW. We used a power of 6-12 mW. We used an FDCA built following the method of (DeVitre *et al.*, 2021) with an extended upper pressure limit from 35 to up to 68 MPa (through use of a sapphire window instead of fused silica-quartz) to produce calibration equations relating CO₂ density and Δ_{CO_2} for our instrument. These equations are available in DiadFit (Wieser and DeVitre, 2023) and have the same functional form as those reported in (DeVitre *et al.*, 2021) with updated coefficients.

Spectra for FI were collected at 37 °C, with temperature regulated at 37°C using a Peltier thermoelectric stage with a center hole fixed on a magnetic aluminum holder. Spectra were acquired with five accumulations of 45 s of integration time (total analytical time = 225 s) in a single window using 1800 grooves/mm (~0.54 cm⁻¹ spectral resolution) and a spectral center of 1325 cm⁻¹. We discarded spectra with less than 3 points above the background (these yield spurious fits with up to >100% error on fitting), those with high backgrounds interfering with the fit and those with normalized Intensity/FWHM <200 according to the criteria of (Yuan and Mayanovic, 2017) as these cannot be fit confidently. A filtered total of 124 FI yielded results with 1 σ in CO₂ density better than ~0.02 g/mL (Data Table S-1)

Neon (Ne) spectra were collected every ~10-15 minutes using the same grating and spectral center as the unknown and three accumulations of 45 s integration time, to correct for non-linearity of the Raman shift axis (Lin *et al.*, 2007; Wang *et al.*, 2011; Lamadrid *et al.*, 2017; DeVitre *et al.*, 2021).

All spectra were processed using Python tool DiadFit v0.0.62 (Wieser and DeVitre, 2023). Spectra are baseline-subtracted prior to fitting (2nd degree polynomial baseline subtraction anchored on either side of peak of interest), and we fit a Pseudo-Voigt peak (mixed Gaussian and Lorentzian model) on each main CO₂ peak (1285 cm⁻¹ and 1389 cm⁻¹). Voigt and Pseudo-Voigt functional forms are typically considered the most appropriate for symmetric Raman peaks (e.g., single-phase CO₂ peaks and Neon emission lines, (Yuan and Mayanovic, 2017)). For fitting, CO₂ spectra were separated into 3 groups based on overall intensity of the spectra, and overlap between main peaks, hot bands (1270 cm⁻¹ and 1410 cm⁻¹) and ¹³C (1370 cm⁻¹) such that additional peaks were simultaneously fit when needed to reduce the effect of residuals on the fit (Jupyter lab notebooks are included in the supplement). We correct our data following the methods of (Lamadrid *et al.*, 2017; DeVitre *et al.*, 2021) using two known Ne emission lines (1115.9919 cm⁻¹ and 1446.4696 cm⁻¹) that encompass the Fermi diad. A single Voigt peak is fit at 1446-1453 cm⁻¹ for the upper line while two Voigt peaks (1113-1120 cm⁻¹ and 1115-1122 cm⁻¹) are used for the lower line since it appears as a double-peak at out spectral resolution. We calculate the instrumental drift correction factor Ne_{coeff} as shown in Eq. 1):

$$Ne_{coeff} = \left(\frac{\Delta Ne_{known}}{\Delta Ne_{observed}} \right) \quad (1)$$

where ΔNe_{known} is the theoretical separation of the Ne emission lines in air and $\Delta Ne_{observed}$ is the measured separation of the same Ne emission lines on the Raman spectrum.

We then model the instrumental drift during each session as a polynomial function (typically 1st to 3rd degree polynomial, unless large temperature fluctuations happened during the session) relating Ne_{coeff} to time in seconds. Exact timestamps are extracted for each CO₂ spectrum and the appropriate Ne_{coeff} from the model is applied to correct the separation of the Fermi Diad. We also fit and calculated areas for SO₂ and CO₃ when observed on the spectra, these are fit as gaussian functions.

We calculate densities using the appropriate calibrated density equations for our instrument using DiadFit (Wieser and DeVitre, 2023). We estimate entrapment temperatures from the Fo content of the olivine (see below). We then calculate pressures from measured densities and estimated entrapment temperatures using the EOS of (Span and Wagner, 1996) and propagate uncertainty using Monte Carlo simulations. Finally, we calculate the depths of entrapment using the crustal density model of (Ryan, 1987), described in (Lerner *et al.*, 2021) for Hawai'i.

1.3 Microthermometry of FI

For samples with bulk CO₂ densities above the critical density of CO₂ (~0.44 g/mL), we conducted micro thermometry experiments to obtain the freezing and homogenization temperatures and calculate an independent estimate of the CO₂ density of the FI. It was not possible to obtain microthermometric data for FI that homogenize to vapor, as it is difficult to observe the homogenization of the thin liquid film into vapor in our samples. These experiments were conducted using a Linkam THMSG600 heating and freezing stage, with environmental control from -195 °C to 600 °C, equipped with a liquid nitrogen cooling pump allowing for cooling rates from 0.01 to 150 °C/min. We used pure CO₂-H₂O standards to calibrate temperature. All experiments were done using the cycling technique (Hansteen and Klügel, 2008) to ensure that homogenization was completed. We then converted the homogenization temperatures to CO₂ density using the EOS of (Span and Wagner, 1996) implemented in DiadFit (Wieser and DeVitre, 2023). All FI were found to have melting temperatures $-56.5 \text{ °C} \pm 0.1 \text{ °C}$ (Fig. S-1a), indicating that they are pure CO₂.

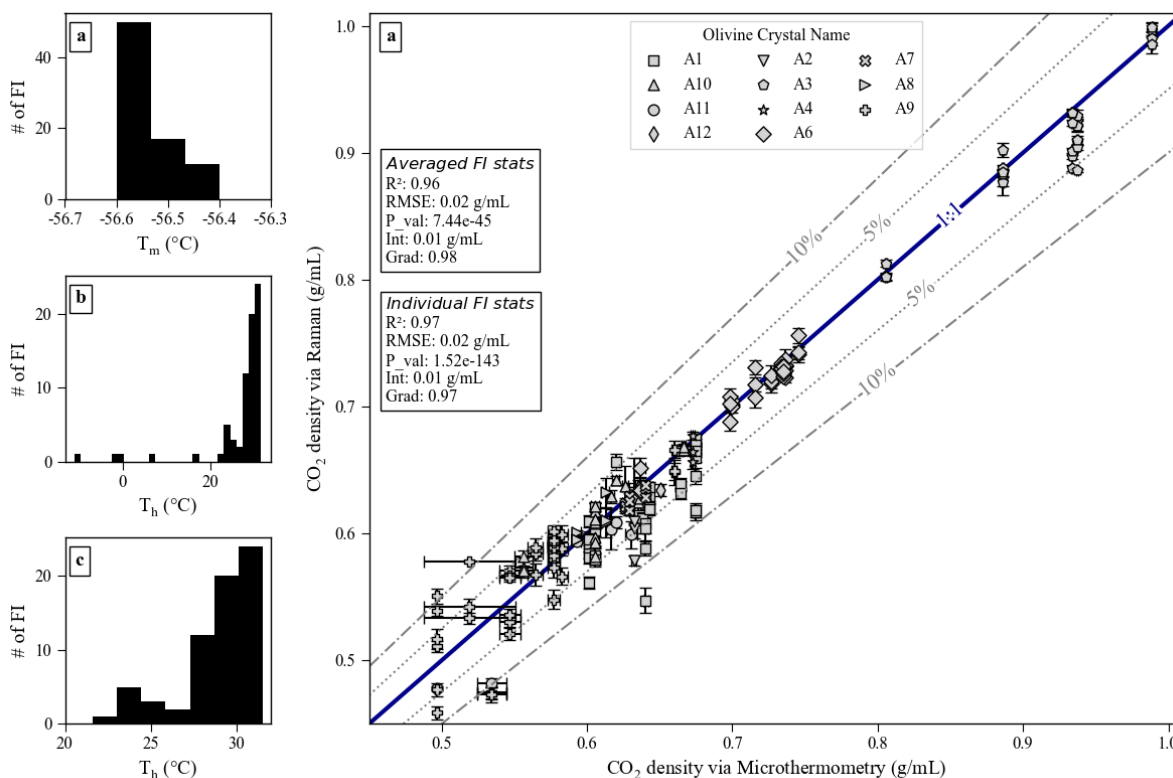


Figure S-1 CO₂ densities via microthermometry versus calibrated Raman Spectroscopy. (a) Freezing temperatures of FI. (b) Homogenization temperatures of FI (all FI homogenized to liquid). (c) close-up of panel b (d) Density via Raman vs density via micro thermometry. FIs in the same crystal are plotted with the same symbol. Error bars for Raman-based CO₂ densities are propagated fitting + Neon correction uncertainties while error bars for microthermometry are the standard deviation of homogenization temperatures obtained during cycling.

Under Raman spectroscopy, none of the FI analysed had detectable amounts of any other gases, however they contained variable amounts of carbonate. Homogenization temperatures ranged from $-11.1 \pm 0.2 \text{ °C}$ to $31.6 \pm 1 \text{ °C}$ (Fig S-1b-c), measurements with homogenization temperatures close to critical were more difficult to perform and the uncertainty on the temperature is therefore higher, limited by the high $\Delta\rho/\Delta T$ and the accuracy of the temperature controller of the stage. Peak-fitting and drift and precision account for most of the uncertainty for Raman (See Fig. 8, Wieser and DeVitre, 2023), while the uncertainty for microthermometry can be attributed to difficulty in observing the phase homogenization near and/or below

the critical density of CO₂, thermocouple accuracy and precision of thermal control. For densities close to critical (~0.44 g/mL), the uncertainty on microthermometry measurements significantly increases due to much higher $\Delta\rho/\Delta T$ – such that very small uncertainties in the homogenization temperature can cause much larger uncertainties in the density (Hansteen and Klugel, 2008).

1.4 Host olivine chemistry

Spot analyses of host olivines were conducted using a JEOL JXA-8230 EPMA in the Mineral and Microchemical Analysis Facility at Stanford University. Counting statistics and other analytical conditions along with repeated analyses of secondary standards (San Carlos Olivine, Stillwater olivine; (Jarosewich *et al.*, 1980)) are presented in the Supporting Information (Data Table S-1).

Entrapment temperatures were estimated from the host olivine Fo content by developing an olivine-only thermometer suitable for Kilauea. The Fo content of an olivine is a function of the MgO and FeO_T content of the liquid from which it equilibrates with, the Ol-Liq partition coefficient, and the proportion of Fe³⁺ in the liquid. Fortunately, Ol-saturated liquids at Kilauea have a relatively constant FeO content (See Fig. S-2, compiled glass data from (Clague and Bohrsen, 1991; Clague *et al.*, 1995; Helz *et al.*, 2014, 2015; Sides *et al.*, 2014a, 2014b; Wieser *et al.*, 2019, 2021). Thus, if the Fo content is known, the K_D is known, the Fe³⁺ ratio is known, and the FeO_T content can be relatively constant, the Fo content can be related to MgO, which in turn, can be related to temperature at Kilauea.

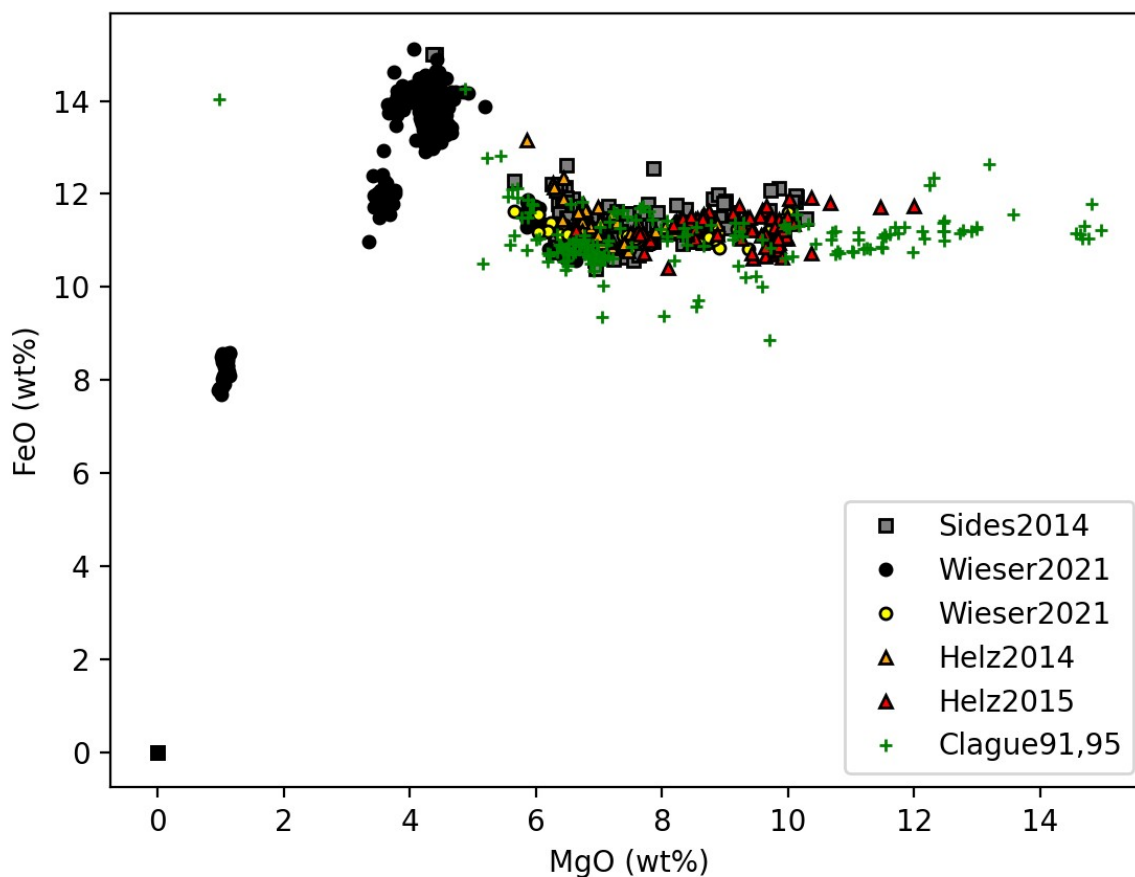


Figure S-2: Compiled glass data used to calibrate an Ol-only thermometer.

To calibrate the Ol-only thermometer, we calculate a liquid-only temperature using the new MgO-thermometer of (Shea *et al.*, 2022) for each liquid in our compiled dataset. We also calculate an equilibrium olivine content using the K_D model of (Shea *et al.*, 2022), assuming $Fe^{3+}/Fe_T=0.15$ (Moussallam *et al.*, 2016; Helz *et al.*, 2017; Lerner *et al.*, 2021). We then fit a 3rd degree polynomial between temperature and Ol Fo content (Fig. S-3). We also show the polynomial that would result from using $Fe^{3+}/Fe_T=0.2$ instead. This is well within the ± 50 K uncertainty used for temperature for the Monte-Carlo simulations (red dashed lines).

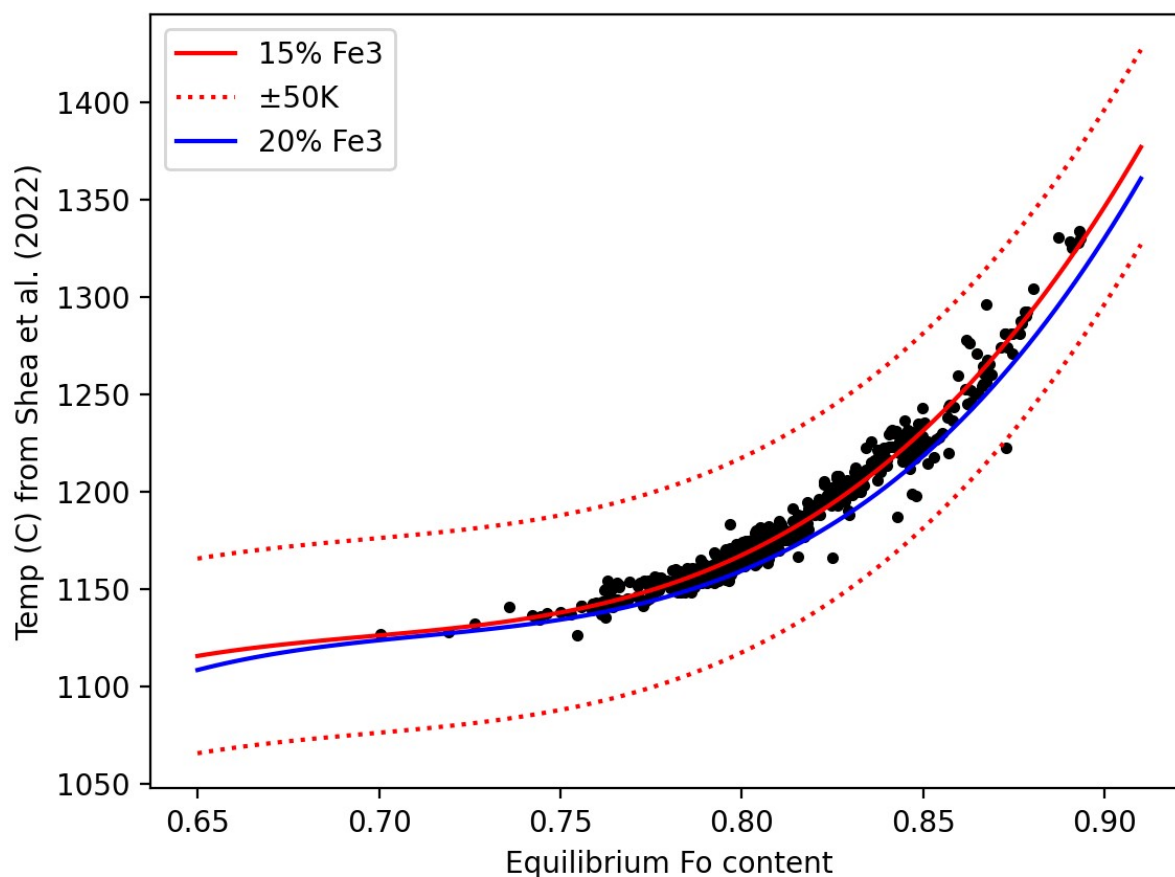


Figure S-3: 3rd degree polynomial fitted between equilibrium Fo content and temperature calculated from the glass composition using the thermometer of (Shea *et al.*, 2022).

We test the success of this Ol-only thermometer on the experimental data used to calibrate the expressions of (Shea *et al.*, 2022). We note that these experimental liquids have far more diversity in FeO content than natural Kilauea liquids, which explains the larger discrepancies that exist. If we restrict comparison to liquids within the mean $\pm 1\sigma$ of the observed distribution of Kilauean liquids, we can see the method is successful within the ± 50 K uncertainty allocated for Monte Carlo methods (pink box, Fig. S-4).

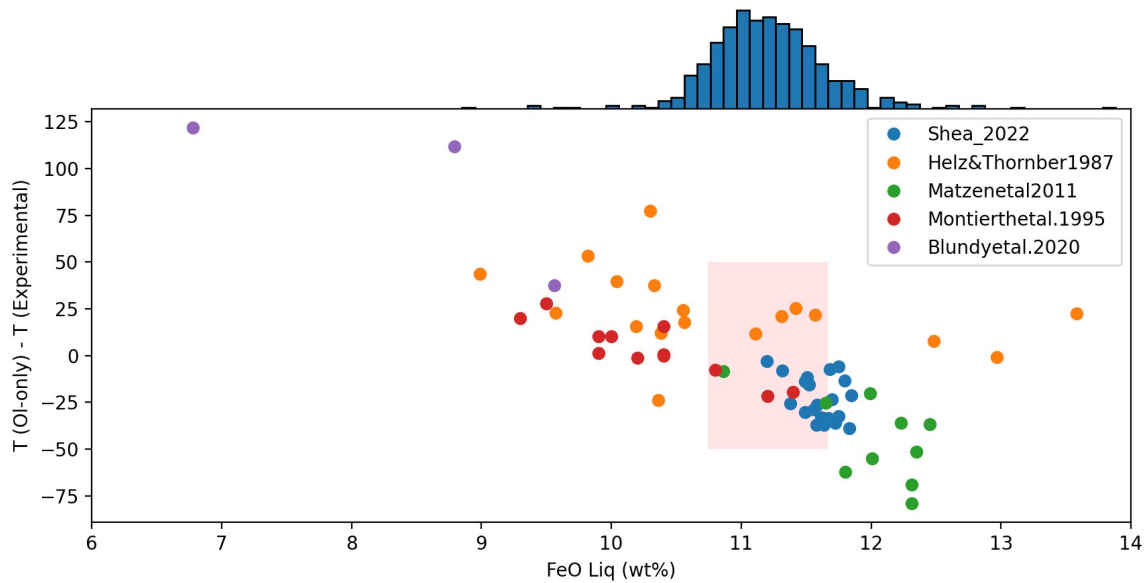


Figure S-4: Assessing the Ol-only thermometer on the calibration dataset of (Shea *et al.*, 2022). The distribution of FeO contents in natural Kilauea liquids is shown with the blue histogram. In the red shaded box, we highlight experimental liquids within the mean \pm 1 σ of this distribution. These experiments lie well within the 1 σ =50K uncertainty allocated for entrapment temperatures.

1.5. Quantifying uncertainty in fluid inclusion pressures

Uncertainties on fluid inclusion pressures are propagated in DiadFit, using Monte Carlo simulations considering 50 K uncertainty on the Temperature and 1 σ uncertainty on density from peak-fit uncertainties on CO₂ spectra and the uncertainty in the Ne correction model estimated by DiadFit

1.6. Estimating SO₂/CO₂ ratios in FI

To estimate the SO₂ fraction in our FI, we calculated the area under the SO₂ peak (\sim 1151 cm⁻¹). We first background subtracted using the same method as for CO₂ and Neon spectra and then fit a spline to the SO₂ spectrum. We then calculated the SO₂ mol % in the FI using the method of (Burke, 2001). We assumed the same instrument efficiency and use the coefficients presented in (Burke, 2001) for CO₂ and SO₂,

2. Statistical significance of the MI vs FI recorded pressures

To assess whether the pressures recorded by MI and FI are statistically different, we conducted Kolmogorov–Smirnov tests (KS). Given the relatively small sample set sizes (N<50), we perform both sample KS tests and Monte-Carlo KS tests using a Python3 routine in which we resampled 1000 times considering the uncertainties of each independent measurement. We compare the MI distributions for MI saturation pressures calculated using 5 different volatile solubility models (MagmaSat, Shishkina, MafiCH, VolatileCalc and Iacono-Marziano(Newman and Lowenstern, 2002; Iacono-Marziano *et al.*, 2012; Shishkina *et al.*, 2014; Ghiorso and Gualda, 2015; Allison *et al.*, 2022)) with the pressure distribution from our new FI data (Fig. S-

5). We note that there are very large variations in the MI saturation pressures when using different solubility models, which by themselves can largely account for the difference in the distributions. If one considers the MagmaSat solubility model, while the sample KS statistics appear significant (which would suggest that the FI are underestimating the magma storage pressures), when we consider the uncertainty on both the FI and particularly the MI measurements, the Monte-Carlo KS statistic is no longer significant for any of the 3 events. This suggests that the FI are predicting the same entrapment pressures as the MI, within the uncertainty of the measurements. Selecting a different solubility model, such as Volatile Calc, or Shishkina.

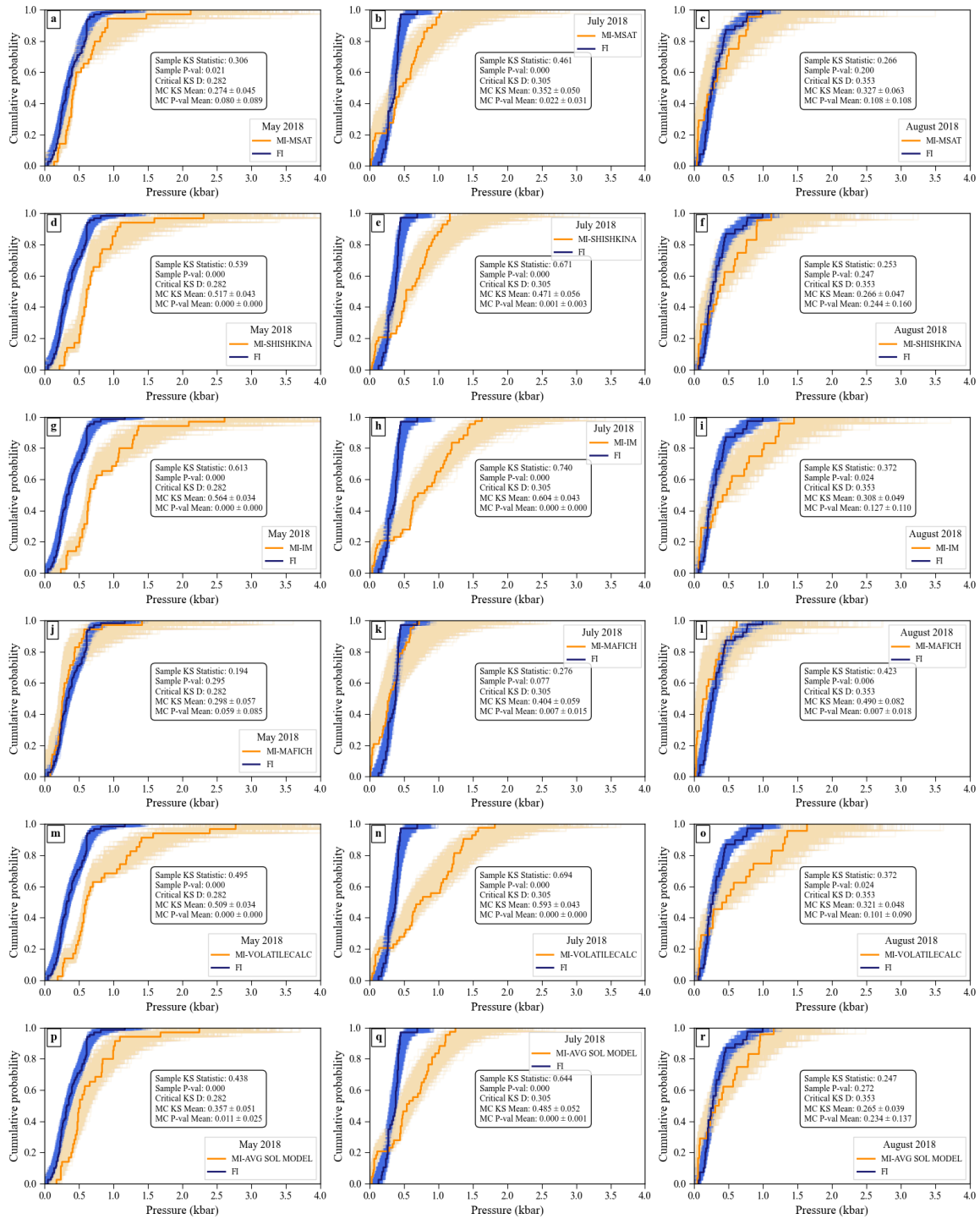


Figure S-5: Monte-Carlo KS tests on Cumulative distributions of pressures for FI (blue) and MI (orange) using different solubility models for each eruptive event. (a-c) MagmaSat. (d-f) Shishkina. (g-i) Iacono-Marziano. (j-l) MafiCH (m-o) VolatileCalc (p-r) Average Solubility model.

3. Fluid % effect on calculated densities and pressures

Magmatic FI are often trapped with variable small amounts of silicate melt. We estimated the proportion of exsolved fluid to silicate melt using FIJI (Schindelin *et al.*, 2012). We filtered out of the dataset any inclusion <80% exsolved fluid. In Fig S-6, we plot the measured CO₂ density of FI in the same crystals, which have variable amounts of exsolved fluid. We also individually plot the FI in each crystal in subsequent panels. We found no clear trends indicating that FI with small amounts of silicate melt (<20%) are likely to record the same conditions as those with nearly no melt at all. Some crystals show a weak relationship where FI with no melt or very little melt have record the highest densities. However, we recognize the dataset is much too small to conclude on this matter. Future work is required to constrain whether any significant relationship exists. For this study, we consider that FI with >80% exsolved fluid offer a suitable record of pressure. This is consistent with previous work indicating that exchange of CO₂ with the melt is negligible in inclusions that trap predominantly the vapor phase (little melt) (Steele-MacInnis *et al.*, 2017).

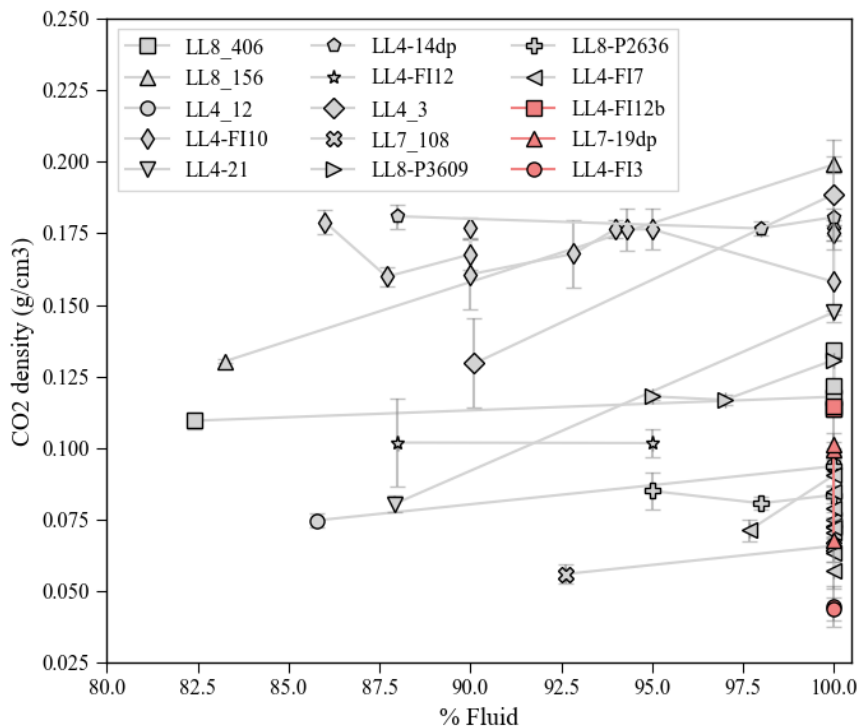
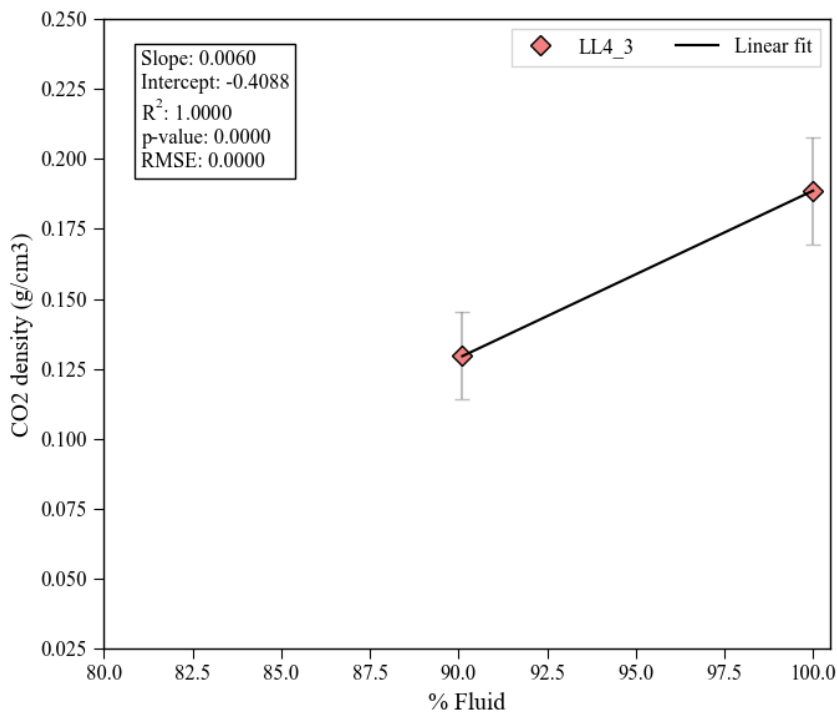
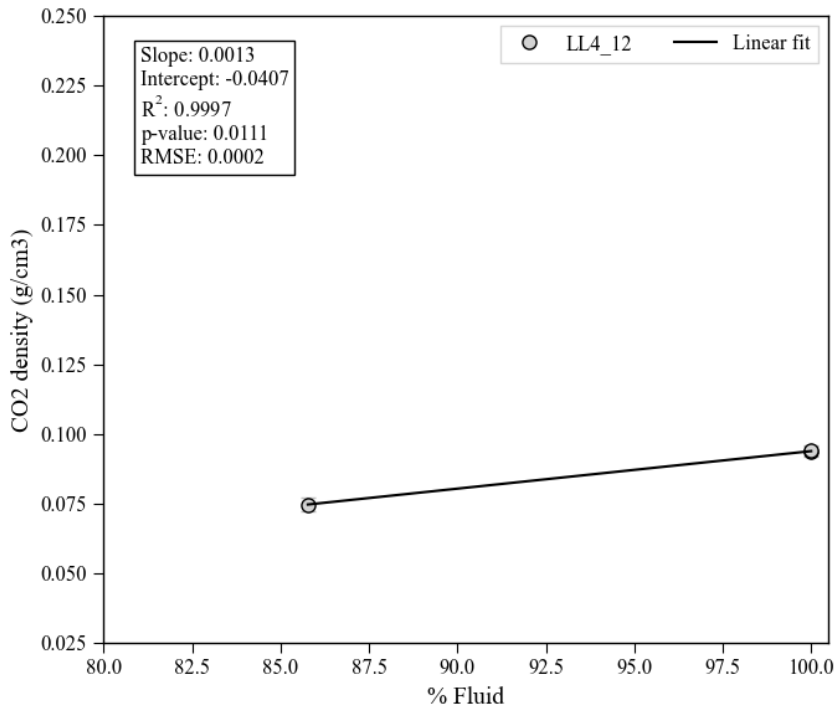
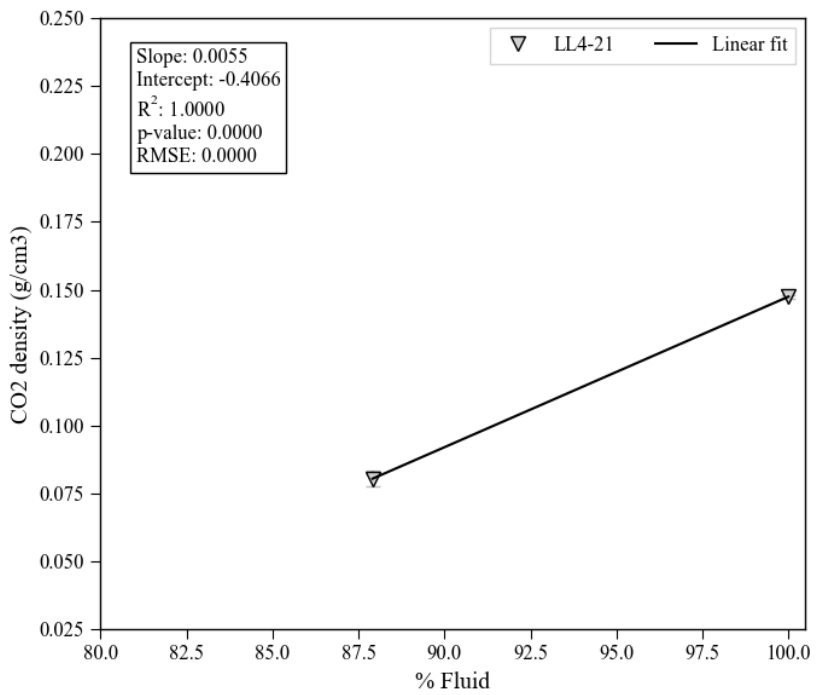
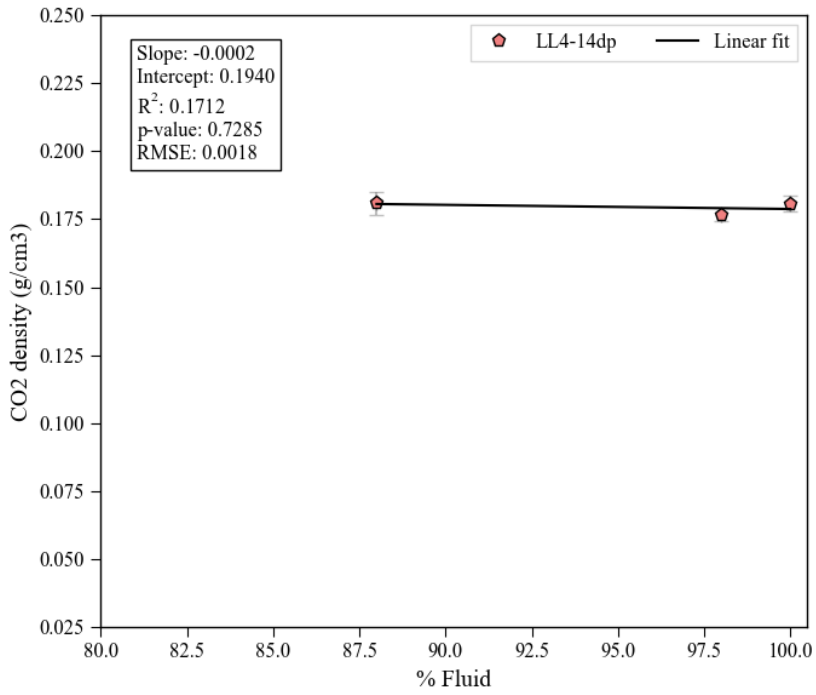
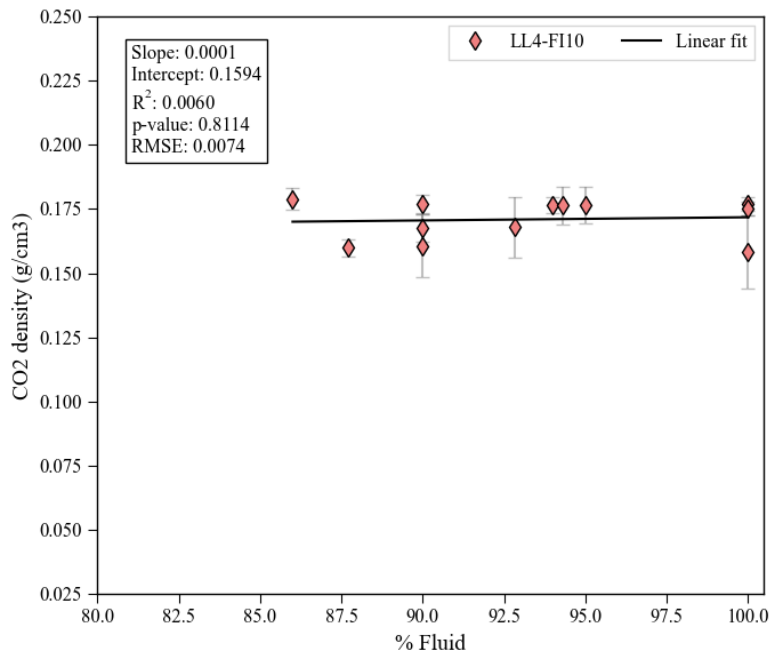
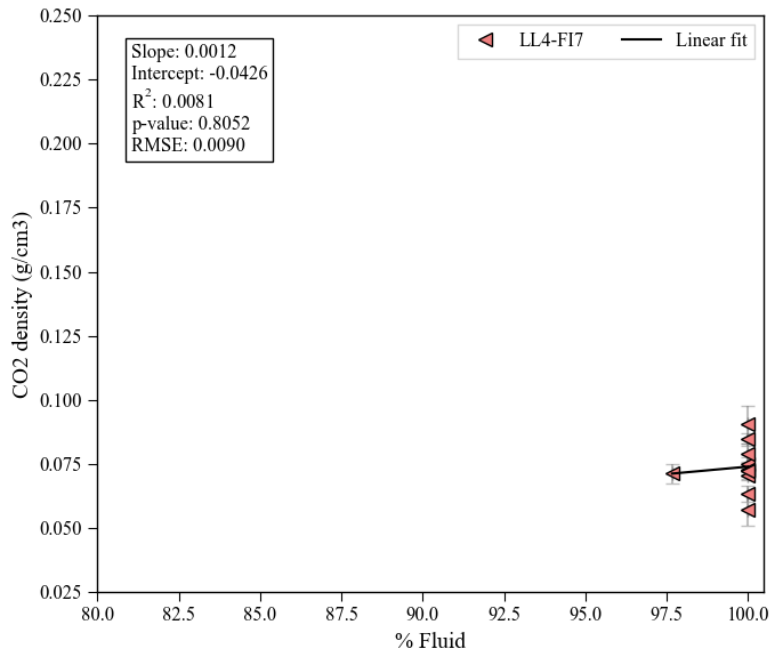


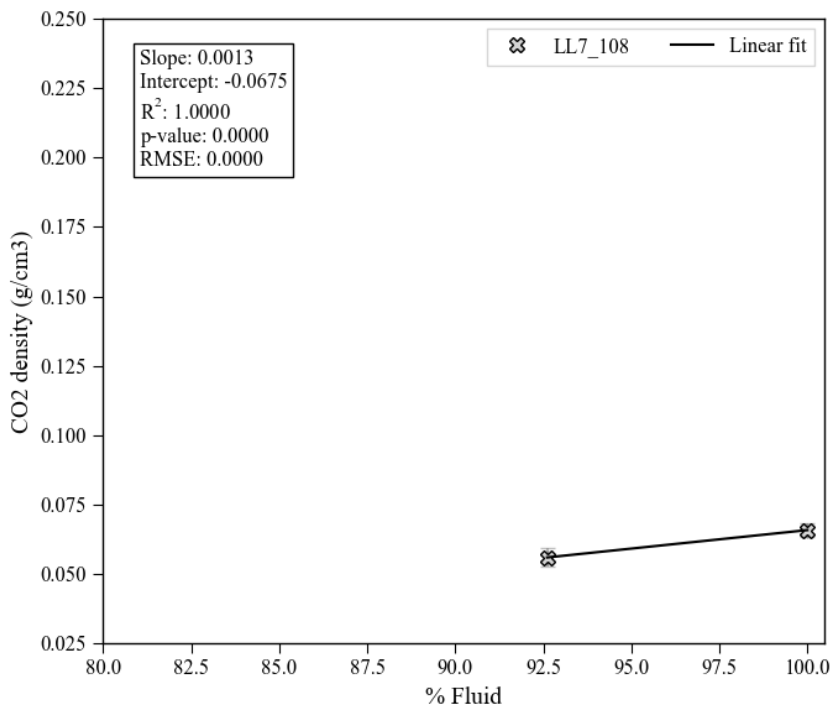
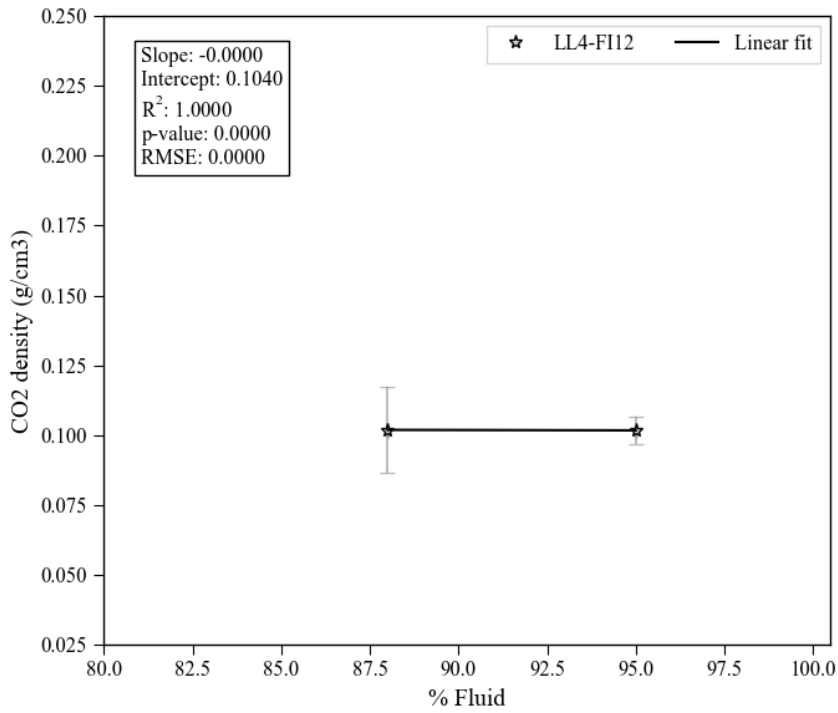
Figure S-6: Measured CO₂ density of FI against the % exsolved fluid for FI “pairs” – these are FI found in the same crystals and relative proximity to each other with apparently similar genetic relationships.

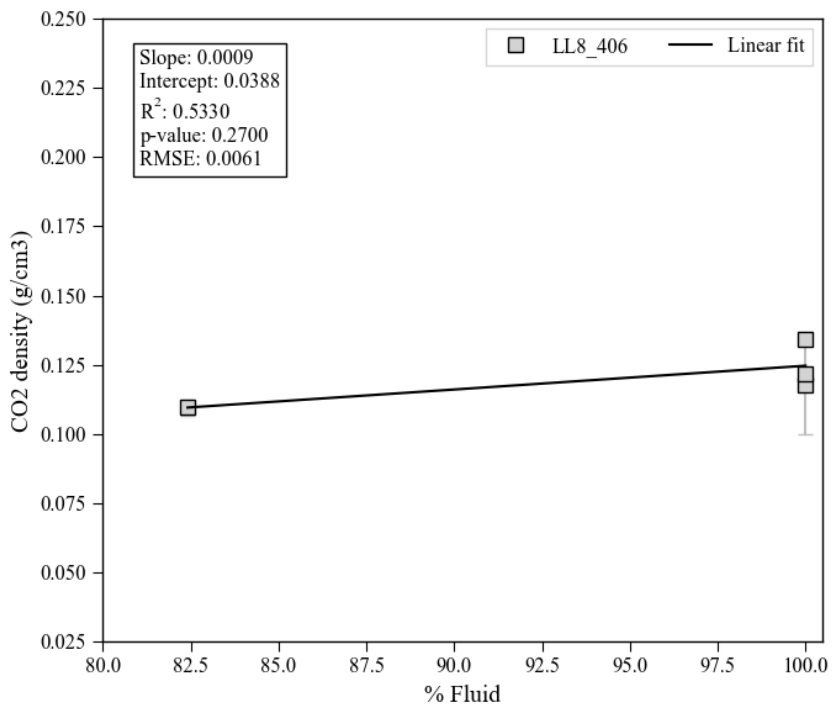
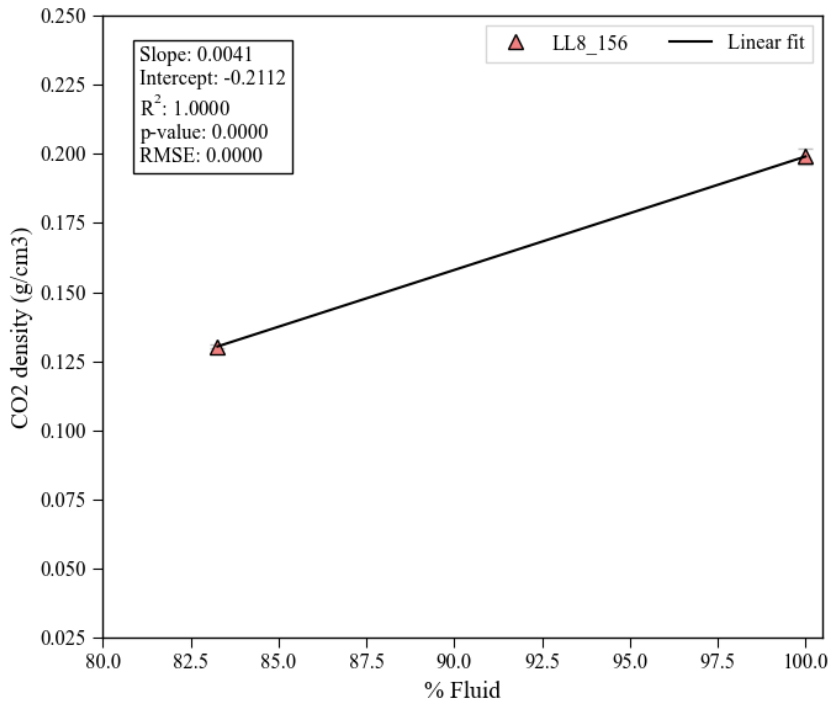
Figure S-6 Part 2: Single crystal plots (Pages 12-18)

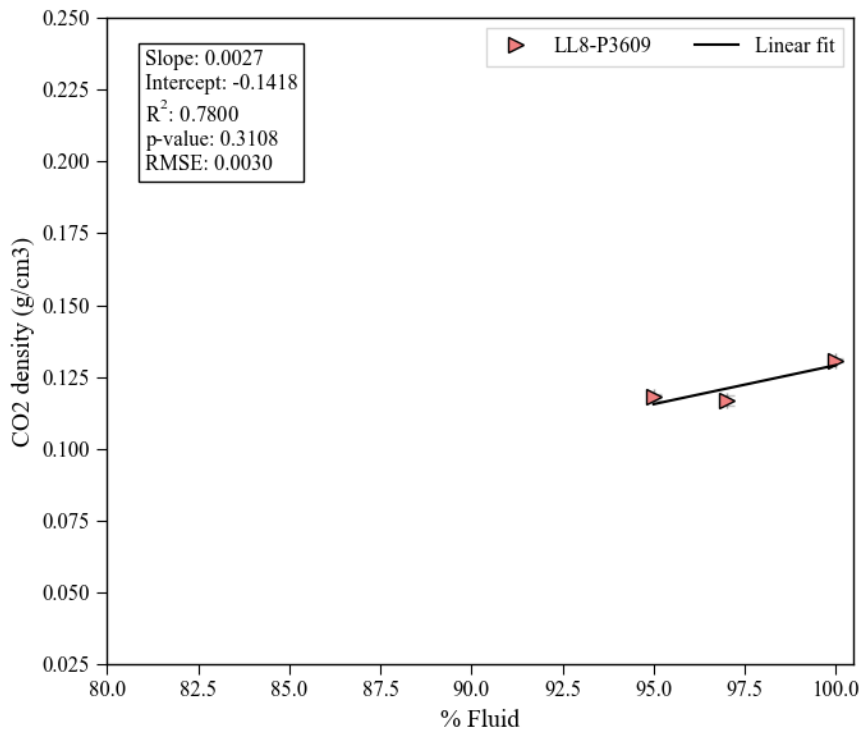
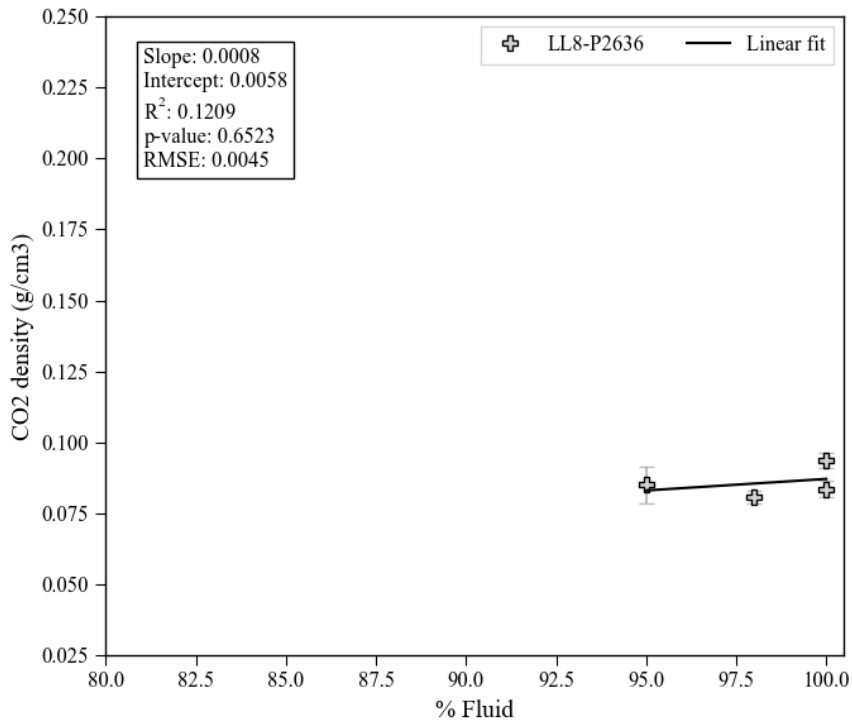












Supplementary information references

Jarosewich, E., Nelen, J.A., Norberg, J.A. (1980) Reference samples for electron microprobe analysis. *Geostandards Newsletter*. Wiley Online Library 4, 43–47.

Ryan, M.P. (1987) The elasticity and contractancy of Hawaiian olivine tholeiite, and its role in the stability and structural evolution of sub-caldera magma reservoirs and rift systems. In *Volcanism in Hawaii. US Geol. Surv. Prof. Pap.* 1350, 1395–1447.

- Clague, D.A., Bohron, W.A. (1991) Origin of xenoliths in the trachyte at Puu Waawaa, Hualalai Volcano, Hawaii. *Contributions to Mineralogy and Petrology*. Springer 108, 439–452.
- Clague, D.A., Moore, J.G., DIXON, J.E., Friesen, W.B. (1995) Petrology of submarine lavas from Kilauea's Puna Ridge, Hawaii. *Journal of Petrology*. Oxford University Press 36, 299–349.
- Span, R., Wagner, W. (1996) A new equation of state for carbon dioxide covering the fluid region from the triple-point temperature to 1100 K at pressures up to 800 MPa. *Journal of physical and chemical reference data*. American Institute of Physics for the National Institute of Standards and ... 25, 1509–1596.
- Burke, E.A.J. (2001) Raman microspectrometry of fluid inclusions. *Lithos* 55, 139–158. [https://doi.org/10.1016/S0024-4937\(00\)00043-8](https://doi.org/10.1016/S0024-4937(00)00043-8).
- Newman, S., Lowenstern, J.B. (2002) VolatileCalc: a silicate melt–H₂O–CO₂ solution model written in Visual Basic for excel. *Computers & Geosciences* 28, 597–604. [https://doi.org/10.1016/S0098-3004\(01\)00081-4](https://doi.org/10.1016/S0098-3004(01)00081-4).
- Lin, F., Bodnar, R.J., Becker, S.P. (2007) Experimental determination of the Raman CH₄ symmetric stretching (ν₁) band position from 1–650bar and 0.3–22°C: Application to fluid inclusion studies. *Geochimica et Cosmochimica Acta* 71, 3746–3756. <https://doi.org/10.1016/j.gca.2007.05.016>.
- Hansteen, T.H., Klügel, A. (2008) Fluid Inclusion Thermobarometry as a Tracer for Magmatic Processes. *Reviews in Mineralogy and Geochemistry* 69, 143–177. <https://doi.org/10.2138/rmg.2008.69.5>.
- Wang, X., Chou, I.-M., Hu, W., Burruss, R.C., Sun, Q., Song, Y. (2011) Raman spectroscopic measurements of CO₂ density: Experimental calibration with high-pressure optical cell (HPOC) and fused silica capillary capsule (FSCC) with application to fluid inclusion observations. *Geochimica et Cosmochimica Acta* 75, 4080–4093. <https://doi.org/10.1016/j.gca.2011.04.028>.
- Iacono-Marziano, G., Morizet, Y., Le Trong, E., Gaillard, F. (2012) New experimental data and semi-empirical parameterization of H₂O–CO₂ solubility in mafic melts. *Geochimica et Cosmochimica Acta*. Elsevier 97, 1–23.
- Schindelin, J., Arganda-Carreras, I., Frise, E., Kaynig, V., Longair, M., Pietzsch, T., Preibisch, S., Rueden, C., Saalfeld, S., Schmid, B., Tinevez, J.-Y., White, D.J., Hartenstein, V., Eliceiri, K., Tomancak, P., Cardona, A. (2012) Fiji: an open-source platform for biological-image analysis. *Nature Methods* 9, 676–682. <https://doi.org/10.1038/nmeth.2019>.
- Helz, R.T., Clague, D.A., Sisson, T.W., Thornber, C.R. (2014) *Petrologic insights into basaltic volcanism at historically active Hawaiian volcanoes. Characteristics of Hawaiian volcanoes*. US Geological Survey, Professional Papers, 237–294.
- Shishkina, T.A., Botcharnikov, R.E., Holtz, F., Almeev, R.R., Jazwa, A.M., Jakubiak, A.A. (2014) Compositional and pressure effects on the solubility of H₂O and CO₂ in mafic melts. *Chemical Geology* 388, 112–129. <https://doi.org/10.1016/j.chemgeo.2014.09.001>.
- Sides, I., Edmonds, M., Maclennan, J., Houghton, B.F., Swanson, D.A., Steele-MacInnis, M.J. (2014a) Magma mixing and high fountaining during the 1959 Kīlauea Iki eruption, Hawai'i. *Earth and Planetary Science Letters*. Elsevier 400, 102–112.
- Sides, I.R., Edmonds, M., Maclennan, J., Swanson, D.A., Houghton, B.F. (2014b) Eruption style at Kīlauea Volcano in Hawai'i linked to primary melt composition. *Nature Geoscience*. Nature Publishing Group 7, 464–469. <https://doi.org/10.1038/ngeo2140>.
- Ghiorso, M.S., Gualda, G.A.R. (2015) An H₂O–CO₂ mixed fluid saturation model compatible with rhyolite-MELTS. *Contributions to Mineralogy and Petrology* 169, 53. <https://doi.org/10.1007/s00410-015-1141-8>.
- Helz, R.T., Clague, D.A., Mastin, L.G., Rose, T.R. (2015) Evidence for large compositional ranges in coeval melts erupted from Kīlauea's summit reservoir. *Hawaiian volcanoes: from source to surface*. Wiley Online Library 125–145.
- Moussallam, Y., Edmonds, M., Scaillet, B., Peters, N., Gennaro, E., Sides, I., Oppenheimer, C. (2016) The impact of degassing on the oxidation state of basaltic magmas: a case study of Kīlauea volcano. *Earth and Planetary Science Letters*. Elsevier 450, 317–325.

- Helz, R.T., Cottrell, E., Brounce, M.N., Kelley, K.A. (2017) Olivine-melt relationships and syneruptive redox variations in the 1959 eruption of Kīlauea Volcano as revealed by XANES. *Journal of Volcanology and Geothermal Research*. Elsevier 333, 1–14.
- Lamadrid, H.M., Moore, L.R., Moncada, D., Rimstidt, J.D., Burruss, R.C., Bodnar, R.J. (2017) Reassessment of the Raman CO₂ densimeter. *Chemical Geology* 450, 210–222. <https://doi.org/10.1016/j.chemgeo.2016.12.034>.
- Steele-MacInnis, M., Esposito, R., Moore, L.R., Hartley, M.E. (2017) Heterogeneously entrapped, vapor-rich melt inclusions record pre-eruptive magmatic volatile contents. *Contributions to Mineralogy and Petrology*. Springer Nature B.V., Heidelberg, Netherlands 172, 1–13. <http://dx.doi.org/10.1007/s00410-017-1343-3>.
- Yuan, X., Mayanovic, R.A. (2017) An Empirical Study on Raman Peak Fitting and Its Application to Raman Quantitative Research. *Applied Spectroscopy*. Society for Applied Spectroscopy 71, 2325–2338.
- Wieser, P.E., Edmonds, M., Maclennan, J., Jenner, F.E., Kunz, B.E. (2019) Crystal scavenging from mush piles recorded by melt inclusions. *Nature Communications*. Nature Publishing Group 10, 5797. <https://doi.org/10.1038/S-41467-019-13518-2>.
- DeVitre, C.L., Allison, C.M., Gazel, E. (2021) A high-precision CO₂ densimeter for Raman spectroscopy using a Fluid Density Calibration Apparatus. *Chemical Geology* 584, 120522. <https://doi.org/10.1016/j.chemgeo.2021.120522>.
- Lerner, A.H., Wallace, P.J., Shea, T., Mourey, A.J., Kelly, P.J., Nadeau, P.A., Elias, T., Kern, C., Clor, L.E., Gansecki, C. (2021) The petrologic and degassing behavior of sulfur and other magmatic volatiles from the 2018 eruption of Kīlauea, Hawai‘i: melt concentrations, magma storage depths, and magma recycling. *Bulletin of Volcanology*. Springer 83, 1–32.
- Wieser, P.E., Lamadrid, H., Maclennan, J., Edmonds, M., Matthews, S., Iacovino, K., Jenner, F.E., Gansecki, C., Trusdell, F., Lee, R.L., Ilyinskaya, E. (2021) Reconstructing Magma Storage Depths for the 2018 Kīlauean Eruption From Melt Inclusion CO₂ Contents: The Importance of Vapor Bubbles. *Geochemistry, Geophysics, Geosystems* 22, e2020GC009364. <https://doi.org/10.1029/2020GC009364>.
- Allison, C.M., Roggensack, K., Clarke, A.B. (2022) MafICH: a general model for H₂O–CO₂ solubility in mafic magmas. *Contributions to Mineralogy and Petrology* 177, 40. <https://doi.org/10.1007/s00410-022-01903-y>.
- Shea, T., Matzen, A., Mourey, A. (2022) Experimental study of Fe–Mg partitioning and zoning during rapid growth of olivine in Hawaiian tholeiites. *Contributions to Mineralogy and Petrology*. Springer 177, 114.
- DeVitre, C.L., Gazel, E., Ramalho, R.S., Venugopal, S., Steele-MacInnis, M., Hua, J., Allison, C.M., Moore, L.R., Carracedo, J.C., Monteleone, B. (2023) Oceanic intraplate explosive eruptions fed directly from the mantle. *Proceedings of the National Academy of Sciences*. Proceedings of the National Academy of Sciences 120, e2302093120. <https://doi.org/10.1073/pnas.2302093120>.
- Wieser, P.E., DeVitre, C.L. (2023) DiadFit: An Open-Source Python3 Tool for Peak fitting of Raman Data from silicate melts and CO₂ fluids. EarthArXiv.